ARRCC
Asia Regional Resilience to a Changing Climate

Report

Understanding and quantifying extreme precipitation events in South Asia

Part IV – Current and future RX1day precipitation over Nepal during the Monsoon season

CARISSA Activity 4: Climate services for the water and hydropower sectors in South Asia

October 2022

Delivery Partners:

UKaid from the British people

Met Office

ICIMOD

This study has been produced in partnership with the Met Office, the International Centre for Integrated Mountain Development (ICIMOD) and the Nepal Development Research Institute (NDRI) as part of the UK Aid funded Asia Regional Resilience to a Changing Climate (ARRCC) programme. The study was conducted under Work Package 3: Climate Analysis for Risk Information & Services in South Asia (CARISSA) and was produced by the Met Office, UK.

Lead Authors

Hamish Steptoe, Met Office

Katy Richardson, Met Office

Reviewers and Contributors

Joe Daron, Met Office

The authors also acknowledge valuable discussion and contributions from:

Theo Economou, Cyprus Institute

Contents

1. Introduction

1.1 Aim

This report constitutes Part IV in a series of reports examining extreme precipitation events in South Asia supporting climate services for the water and hydropower sectors and contributes to the Climate Analysis for Risk Information and Services in South Asia (CARISSA) Work Package of the Asia Regional Resilience to a Changing Climate (ARRCC) programme.

This report focuses on RX1day precipitation extremes in Nepal, defined as the maximum daily total precipitation accumulation over a given analysis period. Within the context of hydropower, high precipitation accumulation events over a period of 1 day (and indeed over shorter periods) have the potential to cause damage to hydropower infrastructure. Damage to infrastructure because of precipitation extremes is most often associated with rainfall accumulation occurring in the monsoon season. Further references to precipitation extremes therefore specifically relate to RX1day precipitation accumulations that occur during the Nepal monsoon season, June to September (JJAS). Note that total precipitation includes both liquid and solid (ice) forms.

The report provides estimates of both present-day extremes and future changes in extreme precipitation under the Representative Concentration Pathways RCP4.5 and RCP8.5 for mid-century (2050s) and end-of-century (2080s) periods over Nepal. The results from both sets of analysis are summarised in the final section, with conclusions and recommendations on how the findings can be used.

1.2 Context & Prior Work

To the best of our knowledge, there is very limited prior work examining how precipitation extremes are projected to change under future climate scenarios in Nepal. A study examining the Upper Indus, Ganges, and Brahmaputra River basins (Wijngaard et al., 2017) showed that an increase in the magnitude of climatic means and extremes are likely by the end of the 21st century, and that climatic extremes show a greater increase than climatic means. However, climate data was based on statistically downscaling four selected global climate models (GCMs), (inmcm4, e.g. Volodin et al., 2010) which poorly represents the weather and climatic processes associated with the South Asia monsoon (see Richardson 2021 and Section 3.2 for further details). Rajbhandari et al. (2016) also look at an envelope of four GCMs from the 5th Phase of the Coupled Model Intercomparison Project (CMIP5, Taylor et al., 2012) to examine changes over the Koshi basin and conclude that average JJAS total precipitation will increase by between 10 and 20 % across RCP4.5 and RCP8.5 scenarios, though do not provide analysis on changing extremes..

Of studies that specifically consider the impacts of changing precipitation on the Himalayan hydropower sector, Shirsat et al. (2021) also use an envelope-based approach and examine two ensembles of five GCMs (containing two GCMs rejected in Section 3.2). They show that the uncertainty in projected precipitation changes results in changes to annual average

streamflow of -12 to 15% (RCP4.5) and by -19 to 48% (RCP8.5). In the Bagmati River Basin, Shrestha et al. (2021) look at three regional climate model (RCM) simulations from the Co-Ordinated Regional Downscaling Experiment (CORDEX) South Asia initiative and conclude that precipitation in the wet season will decrease within a range of 0 to -16%, with an associated reduction in hydropower electricity production of up to -13%.

As in previous parts of this series of reports (Richardson, 2021; Steptoe, 2022), our focus is driven by stakeholder requirements, so we analyse the maximum 1-day precipitation (RX1day) that occurs within each Nepal monsoon season over multiple years of the baseline and future climate periods. We acknowledge that this is only part of the hazard analysis required to fully understand the chain of cascading hazards that encompasses flood risk in Nepal (e.g. Maharjan et al., 2021).

The report has two distinct parts, each with their own methodological approach:

- In Section 2, we make a quantitative best estimate of extreme precipitation in the present day climate, based on an analysis of four observations-based data sources (the selection of which is detailed in Steptoe (2022);

- In Section 3, we estimate future changes in extreme precipitation during the monsoon for future periods under RCP4.5 and RCP8.5 scenarios from CMIP5 and CORDEX model simulations drawing on results of the process-based evaluation presented in Richardson (2021).

2. Present-day extreme precipitation

2.1 Methods

Using the four data sets analysed in Steptoe (2022), MSWEP v2.8, HAR v2, IMDAA and GloSea5 N512, we construct a data blending framework based on Generalised Additive Models (GAMs, e.g. Hastie & Tibshirani, 1990; Wood, 2017, 2020) to undertake extreme value analysis of RX1day JJAS block-maxima[a] extreme precipitation , modelled as a Generalised Extreme Value (GEV) distribution:

$$Y_{s,t,m} \sim GEV\left(\mu_{s,t,m}, \sigma_{s,t,m}, \xi_m\right) \quad (1)$$

$$\mu_{s,t,m} = \beta_0 + f\left(year(t)\right) + g\left(lon(s), lat(s)\right) + h(lon(s), lat(s), u_m^{(\mu)}) + \epsilon_i \quad (2)$$

$$\log\left(\sigma_{s,t,m}\right) = \gamma_0 + f(year(t)) + g(lon(s), lat(s)) + h(lon(s), lat(s), u_m^{(\sigma)}) + \epsilon_i \quad (3)$$

[a] A peak-over-threshold approach could also be applied, but we find the block maxima approach convenient to reduce data volumes sufficiently to allow reasonable model fitting time on the available computational resources.

$$logit(\xi_m) = \delta_0 + u_m^{(\xi)} + \epsilon_i \quad (4)$$

where $Y_{s,t,m}$ represents RX1day precipitation extreme observations as a GEV distribution with $\mu_{s,t,m}$ (location), $\sigma_{s,t,m}$ (scale) and ξ_m (shape) parameters, that vary in space (across $lon = [79.63, 88.07]$°E and $lat = [26.37, 30.35]$°N, giving grid cells $s = 1 \dots 450$), time (for $year = [1979, 2020]$, giving $t = 1 \dots 42$) and observational data sets ($m = 1 \dots 4$)[b]. The $Y_{s,t,m}$ GEV is modelled using a hierarchical GAM (e.g. Pedersen et al., 2019) with intercepts $(\beta_0, \gamma_0, \delta_0)$ and selected covariates accounting for long-term variability in time $f(year(t))$, variability in space $g(lon(s), lat(s))$ and model specific deviations $h(lon(s), lat(s), u_m)$ that describe how each individual dataset estimate m deviates from the general spatial field $g(\cdot)$ (referred to as a 'random effect' in some statistical modelling contexts). To simulate uncertainty from unobserved datasets (i.e. imagining we had more than four observed datasets) in $u_m^{(\cdot)}$ group terms, the random (or group) effects are further simulated as:

$$u_m^{(\mu)} \sim Normal(0, \sigma_\mu^2) \quad (5)$$

$$u_m^{(\sigma)} \sim Normal(0, \sigma_\sigma^2) \quad (6)$$

$$u_m^{(\xi)} \sim Normal(0, \sigma_\xi^2) \quad (7)$$

where the uncertainty associated with different observed datasets can be integrated out for each GEV term:

$$\mu_{s,t} = \int_{u_{s,m}^{(\mu)}} \mu_{s,t,m} \; du_m^{(\mu)} \quad (8)$$

so that predictions are finally based on:

$$Y_{s,t} \sim GEV\left(\mu_{s,t}, \sigma_{s,t}, \xi\right) \quad (9)$$

Model fitting was performed using the R package `mgcv` of (Wood, 2003, 2017). Spatial terms are defined as isotropic Duchlon splines (Duchon, 1977; Miller & Wood, 2014) with first derivative penalties that aim to reduce collinearity between the global smoother ($g(\cdot)$) and the group-specific terms ($h(\cdot)$), as detailed in Pederson et al. (2019). Although topography was found to be a significant predictor of extreme precipitation, it was also found to be highly colinear (> 0.9) with the spatial terms. As this can lead to substantial underestimates of the variance of fitted model terms (Ramsay et al., 2003), topographic effects are excluded in the

[b] For GloSea5 data, we use all 24 ensemble members weighting them so that each observation from an individual ensemble member contributes $\frac{1}{24}$ to the model fit. This way the GloSea5 dataset has the same influence on the final model fit as other observational datasets with fewer data points.

final model fit. In the final model predictions, time varying coefficients (i.e. $f(year(t))$ terms) are set to zero, to exclude the long-term RX1day variability.

The smooth model parameters are estimated using restricted maximum likelihood (REML), and we take a Bayesian view of the model as detailed in Wood (2017). We interpret the posterior distribution of extreme precipitation (that incorporates the uncertainty due to differences in the four observed estimates of extremes) in terms of an equal-tailed span of values that are most credible, referred to as the credible interval (CI) based on estimations of the 2.5th and 97.5th percentiles of posterior estimates (Kruschke, 2015). The CI represents the range of extreme precipitation estimates that are most credible given the input datasets. A wide CI represents more uncertainty is the model estimates, which arises from greater disagreements between the observed datasets. A schematic of this hierarchical model is visualised in Figure 1.

Model diagnostic and validation plots can be found in Appendix A. In particular, Figure 25 compares the different model datasets against the GAM model 'best estimate' for 12 randomised grid locations, showing the effect of model fitting based on the 4 datasets.

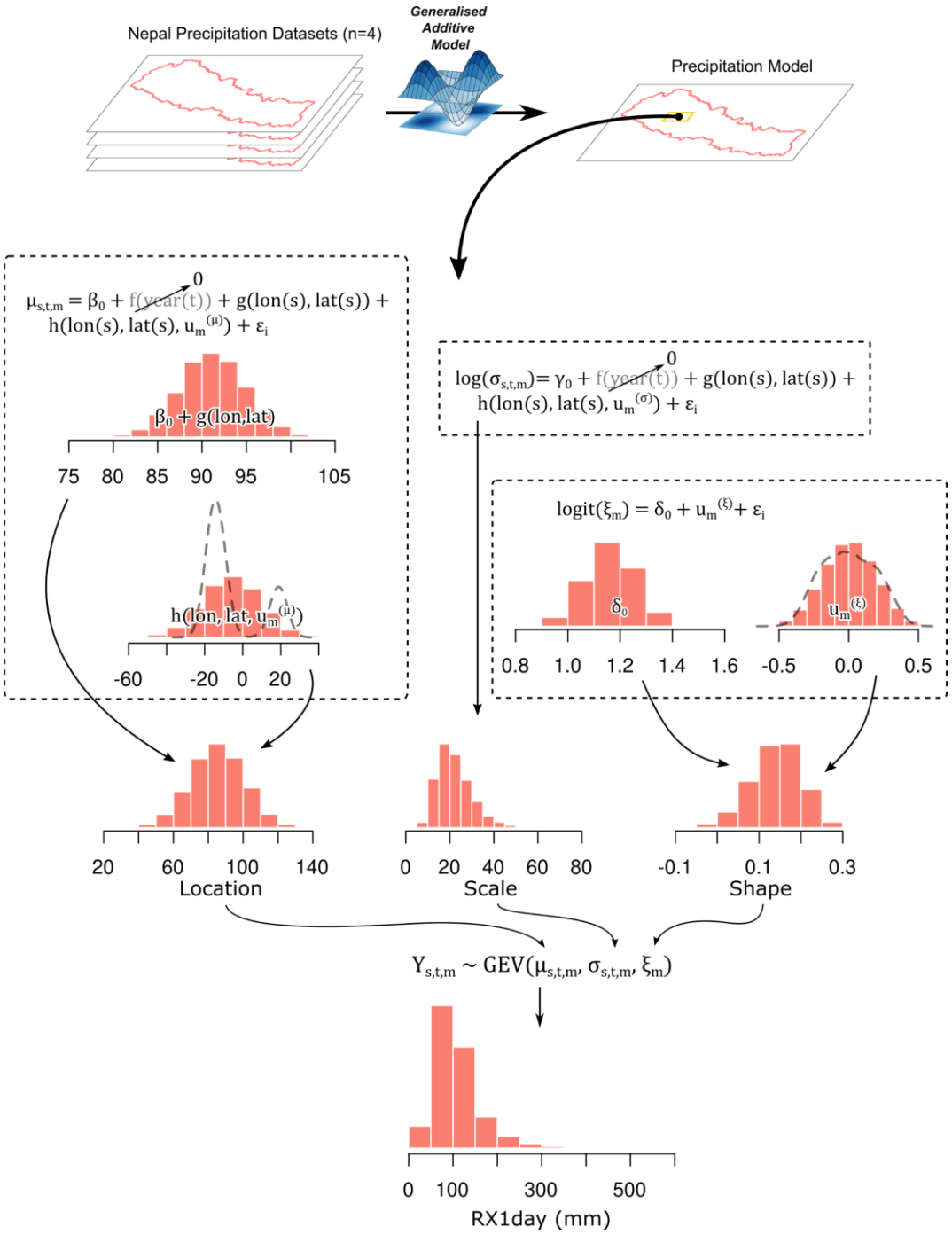

Figure 1 Schematic illustration of the data blending framework based on a hierarchical Generalised Additive Model (GAM). The GAM is used to combine data from four different datasets of extreme precipitation (top) into a single best estimate. At each grid cell the final (posterior) Generalised Extreme Value (GEV) model of $Y_{s,t}$ (Eq. 9) incorporates uncertainty due to spatial variability across each different dataset estimate in the location ($\mu_{s,t,m}$, Eq. 2) and scale ($\sigma_{s,t,m}$, Eq. 3) terms, and model specific estimates of the shape (ξ_m, Eq. 4) parameter. Visualisations of model estimates of location and shape parameters, and the resulting posterior $Y_{s,t}$ estimate are shown in the histograms.

2.2 Best estimate of historical climate extremes

Here we present results of the estimates of present-day precipitation extremes. Using available data, we present the central estimate (50th percentile) and upper-case estimate (99th percentile) for precipitation extremes, and the range of uncertainty in the median (the 2.5 – 97.5th percentile credible interval (CI) range). All estimates represent area averaged precipitation extremes, at the same resolution of the input data: in this case 0.35° x 0.23° (~ 800 km^2).

Figure 2 shows the spatial variability of the RX1day JJAS estimate for return periods of 2, 20 and 100 years. Extreme precipitation is strongly associated with topography, with the Terai areas of Nepal generally seeing greater precipitation extremes than the Himalayan areas. Within the Terai, southern parts of Sudurpashchim, Gandaki, Madhesh and Province 1 have 1-in-2 year RX1day values of 110 – 200 mm (50th – 99th percentile). For 1-in-100-year events, parts of Sudurpashchim may experience RX1day extremes in excess of 350 mm, with Madhesh widely seeing 320 – 350 mm. Uncertainty for the Terai and mountain areas is generally ± 0 – 40% of the median value for 1-in-2 year events, and as expected the level of uncertainty increases with return period. Compared to two other common observed datasets not used in the model fitting (Figure 3), ERA5 (Hersbach et al., 2018) and Aphrodite-2 (Yatagai et al., 2012), the spatial distribution of RX1day values are similar but our best fit blended estimates are uniformly wetter for return periods greater than 1-in-2 years. Figure 25 suggest that higher precipitation values in the blended data tend to be driven by the HAR and IMDAA datasets, both of which have relatively high-resolution source data. The wetter return periods could reflect the improved resolution and the associated microphysics that can be resolved over the complex Nepal topography, especially given that differences between ERA5 and the blended data appear most prominent over the mountain regions (more obvious for lower thresholds).

An alternative visualisation to Figure 2, Figure 4 plots the likelihood of occurrence (in terms of return periods) for given RX1day thresholds. This visualisation shows areas of the same return period for given thresholds as the same colour. These plots show that the Terai and hill regions are likely to see area-averaged RX1day accumulations of 75 mm more-frequently-or-equal-to once every 2 years. For higher thresholds, areas of the Terai still have the potential to experience 100 mm at least every other year. For 140 mm area-averaged RX1day accumulation (which triggers a DHM precipitation warning), there is potential for most Terai areas (including the cities of Dhangadhi, Nepalganj, Siddharthanagar, Birganj and Rajbiraj) to experience this threshold once every 2 – 5 years even in the median estimate.

Comparing these thresholds against ERA5 and Aphrodite-2 (Figures 5 and 6), shows that the blended data uniformly predicts all 3 thresholds to occur at least 100-times more likely than suggested by Aphrodite-2 data alone. Further work is required to identify what causes this substantial difference, but it could be driven by the relatively sparse gauge data coverage that contributes to Aphrodite-2 over Nepal (see Steptoe, 2022). Differences with ERA5 are more complex. Our blended dataset suggests that thresholds of 75 and 100 mm occur more frequently than ERA5 in the Himalayas and some parts of the Terai, but these thresholds are generally reached less frequently that ERA5 in the middle mountains. Looking specifically at the 15 most populated cities in Nepal, Figure 7 shows exceedance probability curves for

a range of RX1day values up to 300 mm. As in Figure 5, Aphrodite-2 exceedance probabilities are uniformly lower than our blended data and ERA5. For low return period (≤ 1-in-5 year events) ERA5 tends to predict greater RX1day values than our blended dataset, but this is quickly overtaken for return periods > 1-in-5 years.

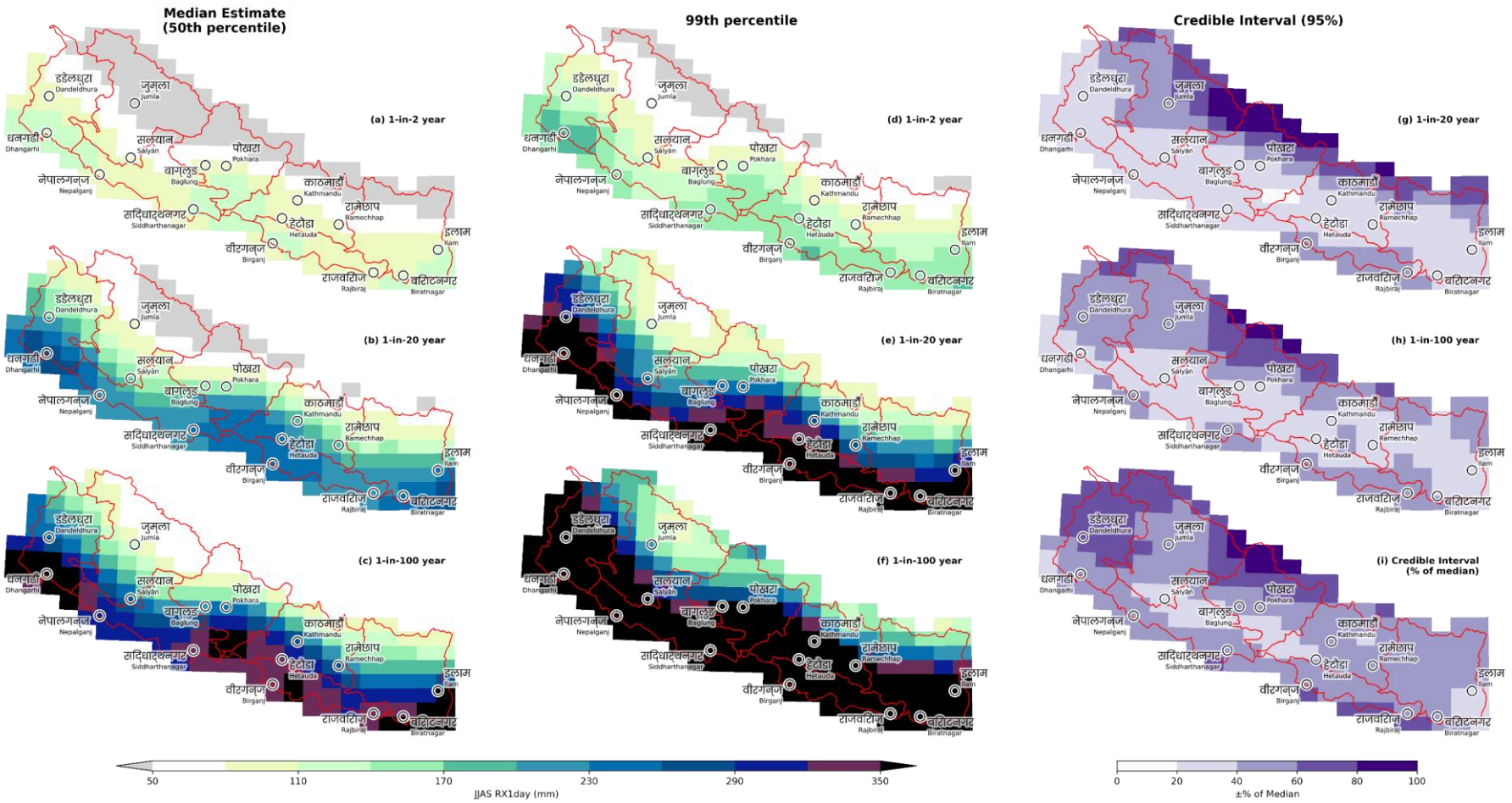

Figure 2 Spatial variability of JJAS RX1day return periods estimates in mm for the median (a-c) and 99th percentile (d-f), and the variability (uncertainty) associated with the prediction at each grid cell standardised as a percentage of the median (g-i). The RX1day estimate at each grid cell is representative of an area average over ~800 km^2. Grid cells with an area average < 50 mm are grey and grid cells ≥ 350 mm are black.

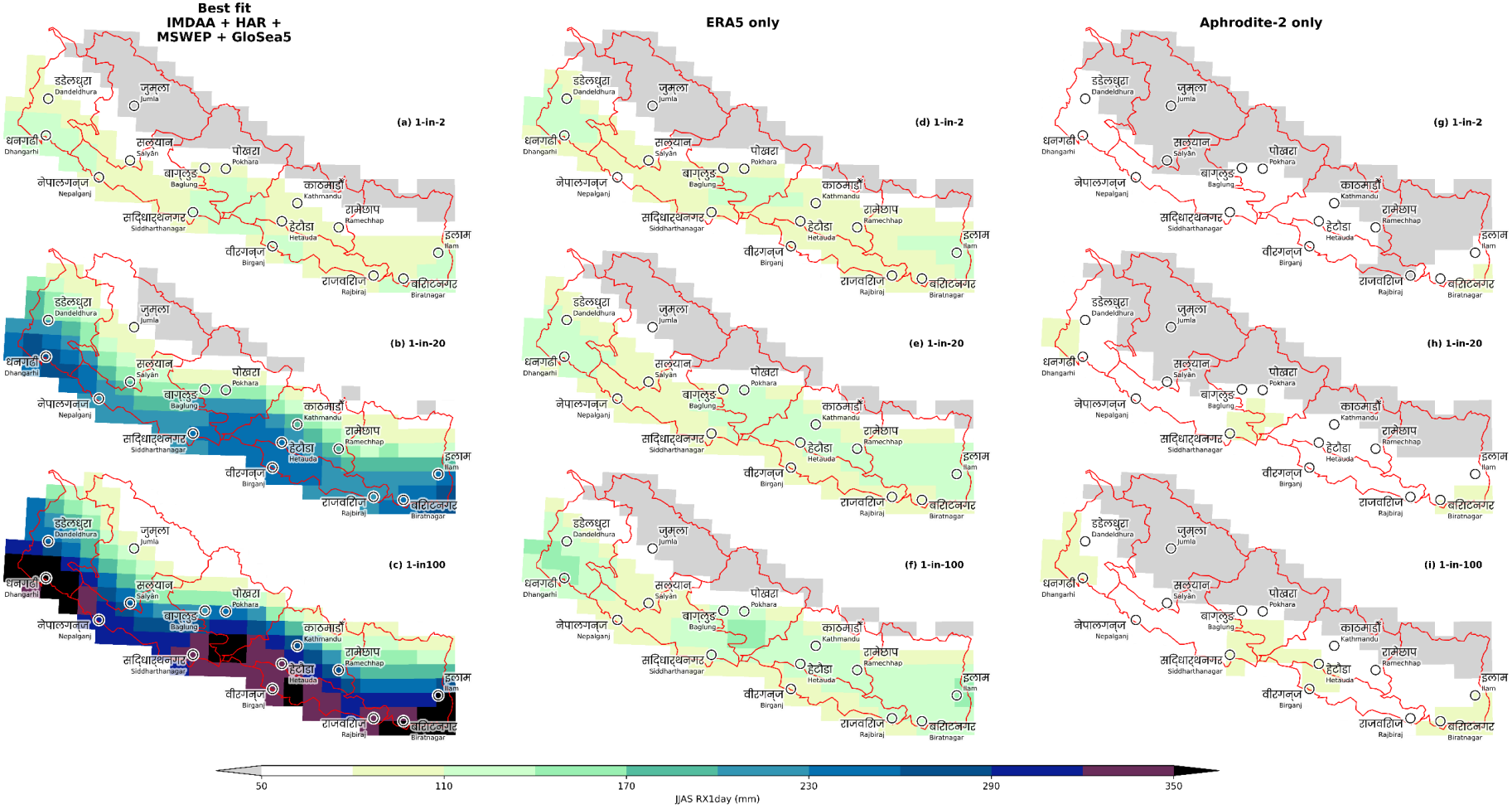

Figure 3 Comparison of spatial variability of median (50th percentile) JJAS RX1day return periods estimates for the best fit blended dataset (a – c, as for Figure 2) against ERA5 (d – f) and Aphrodite-2 (g – i).

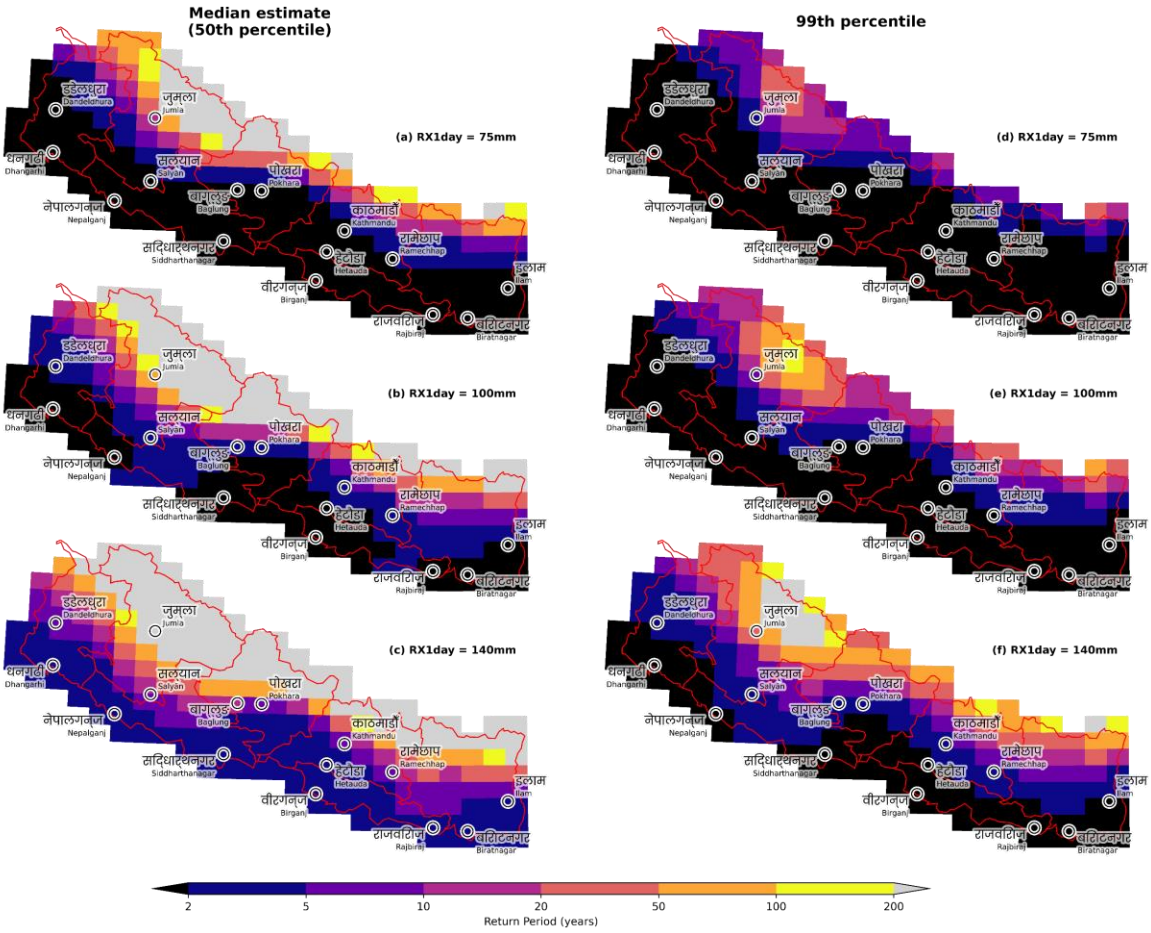

Figure 4 Spatial variability of JJAS RX1day exceedance probability estimates for thresholds of 75 mm (a, d), 100 mm (b, e) and 140 mm (c, f) for median (a – c) and 99th (d – f) percentiles. The return periods estimate at each grid cell is representative of an area average over ~800 km^2.

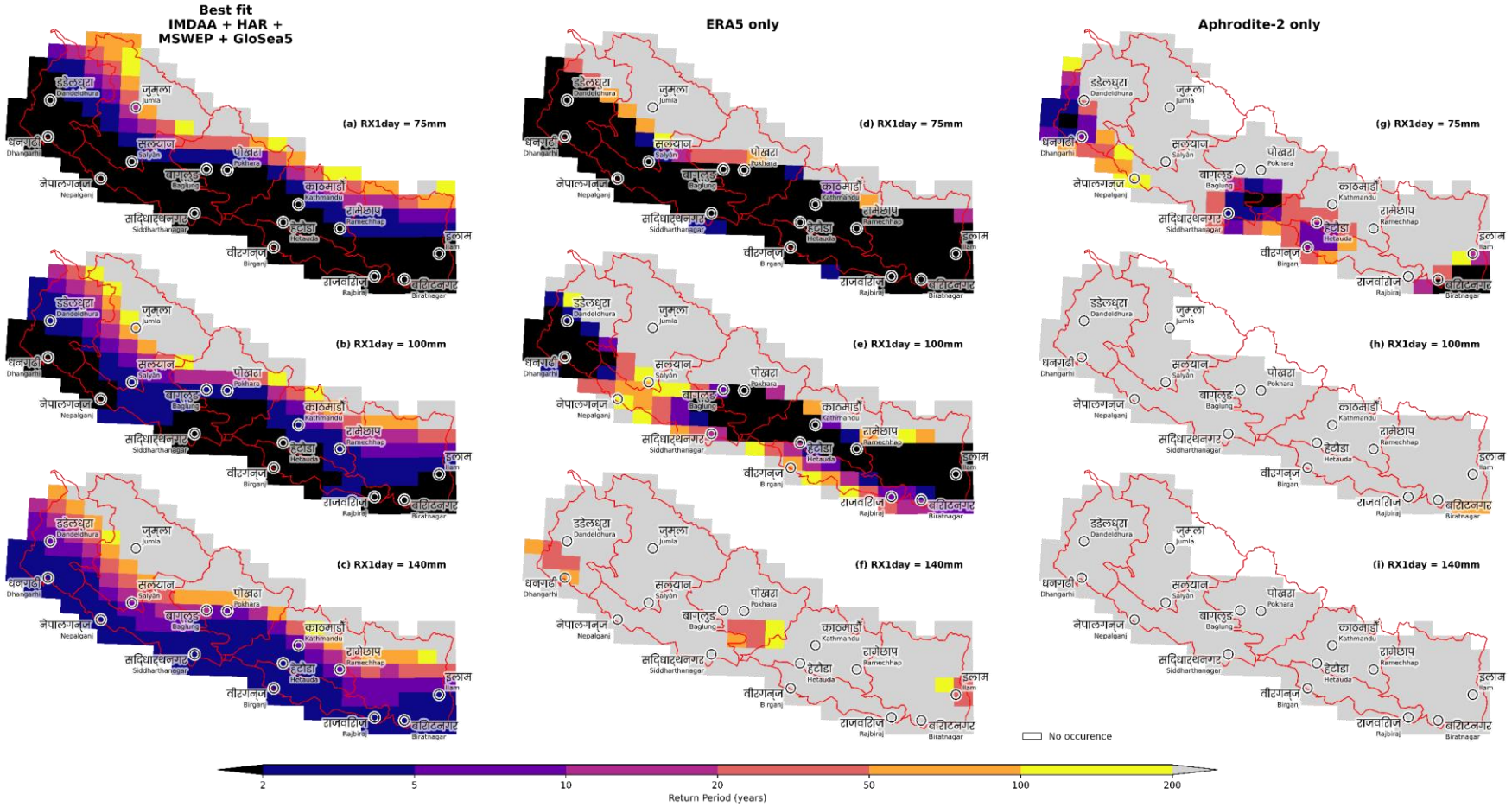

Figure 5 Comparison of median (50th percentile) exceedance probabilities of the best fit blended dataset (a – c, as for Figure 4) against ERA5 (d – f) and Aphrodite-2 (g – i). Where a dataset does not reach a given threshold at any return period (i.e. there is no occurrence, in this figure only Aphrodite-2) the grid cell is left unshaded.

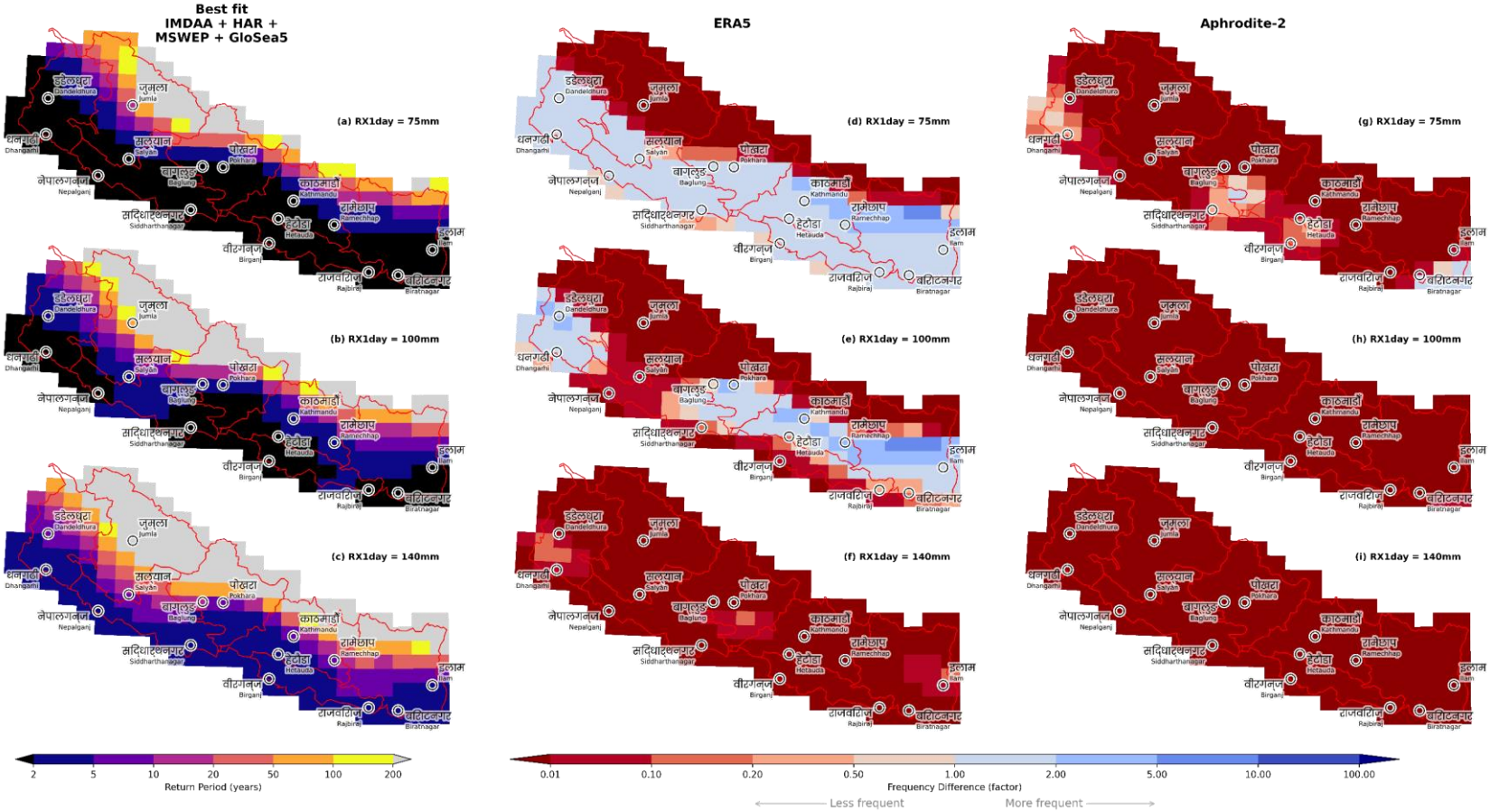

Figure 6 Comparison of median (50th percentile) exceedance probabilities of the best fit blended dataset (a – c, as for Figure 5), but showing the difference in frequency against ERA5 (d – f) and Aphrodite-2 (g – i) as a factor of the best-fit blended data. Frequency differences <1 indicate that the return period for a given threshold is *less frequent* than the blended data. Frequency differences >1 indicate that the return period for a given threshold is *more frequent* than the blended data.

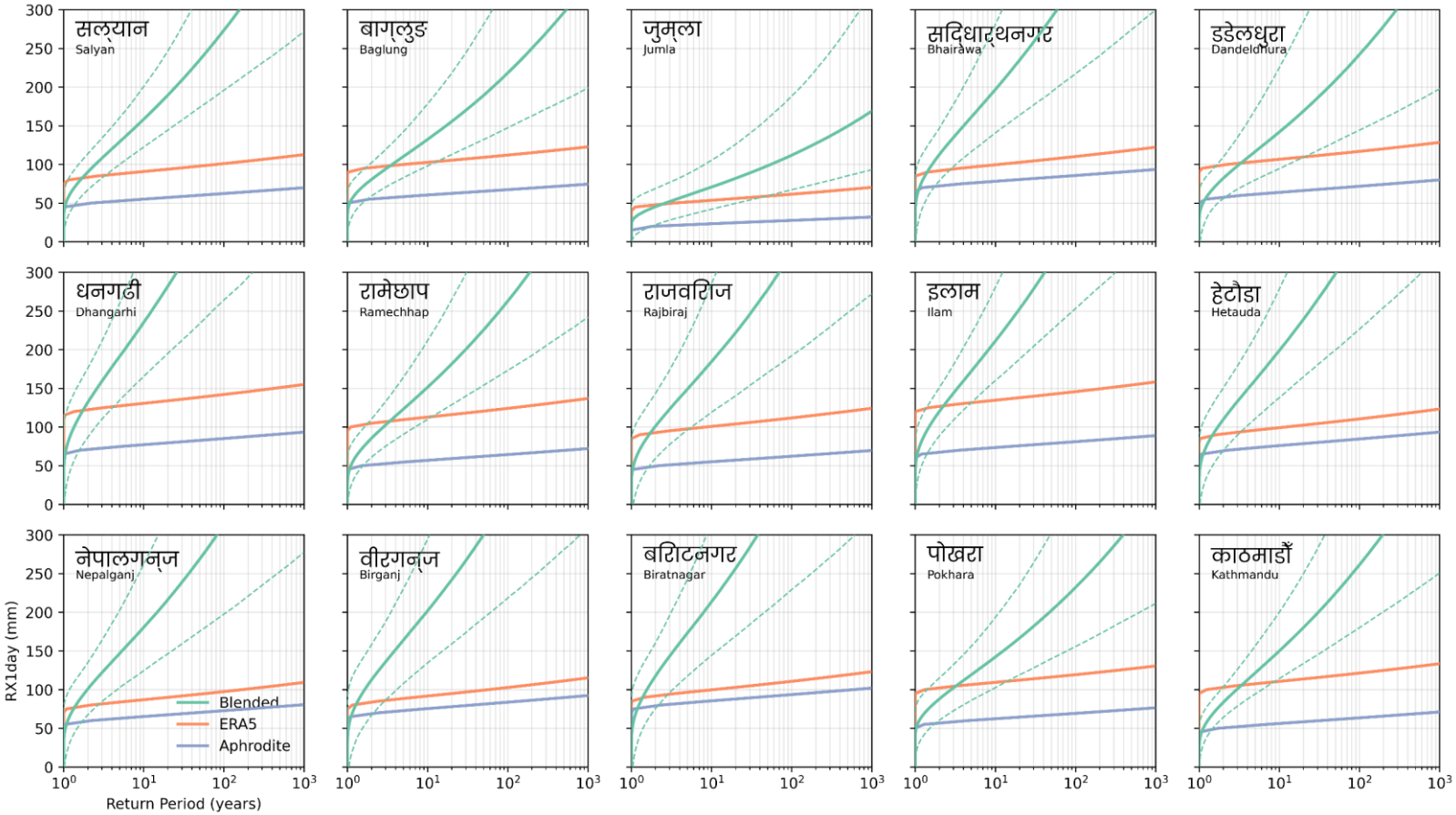

Figure 7 Excedance probability curves for 15 of the most populated cities in Nepal. Return period estimates across a range of JJAS RX1day values from 0 – 300 mm from our blended data set are shown in green with their assocated 2.5th and 97.5th percentile intervals marked as dashed lines. Comparative curves for ERA5 and Aphrodite-2 (regridded to match the best fit blended data resolution) are shown in orange and purple respecitvely. Uncertanty intervals for the ERA5 and Aphdrodite-2 data are not shown, but are an order of magnitdue smaller than for our blended dataset.

3. Future changes in extreme precipitation

A set of plausible scenarios of future change in extreme precipitation during the monsoon season for Nepal have been selected. Here we provide explanation of the selection process and present the scenarios, using analysis of a large ensemble of both GCM and RCM projections. Building on a process-based evaluation, focusing on how well available models simulate the relevant processes that drive extreme precipitation in the region (Richardson, 2021), subsequent analysis aims to provide a representative set of plausible scenarios for extreme precipitation change across Nepal for the 2050s and 2080s under different future greenhouse gas concentration pathways. The scenarios have two key purposes:

1. To provide information about future changes in extreme precipitation in Nepal for communicating with relevant stakeholders.

2. To provide a recommended set of climate model simulations to drive hydrological models (and potentially other climate impact models) to translate changes in extreme precipitation into information about surface run-off, river flow and other hydrological variables.

3.1 Projected changes from an ensemble of global and regional climate model simulations

The model simulations considered in this study include 30 GCM simulations from CMIP5 and 17 dynamically downscaled RCM projections from CORDEX (Giorgi & Gutowski, 2015) for the South Asia domain. The RCM simulations from CORDEX take the output from a subset of the CMIP5 GCMs and provide higher resolution output, better accounting for local factors such as topography. These two ensembles of climate model projections were used to inform the IPCC 5th and 6th Assessment Reports (IPCC, 2013, 2021). Although the more recent CMIP6 model simulations are now available, these were not available at the time of the model evaluation (Richardson, 2021), and the RCMs have not yet been used to downscale the CMIP6 projections.

Figures 8 and 9 show projected changes in the maximum[c] daily precipitation (RX1day) during the JJAS season in Nepal from the 30 CMIP5 GCM simulations and 17 CORDEX WAS-44 model simulations for the 2050s (using 30 years of data from 2041 to 2070), under the RCP4.5 greenhouse gas concentration pathway. Similar maps for the 2080s (using 30 years of data from 2071 to 2100) under RCP4.5 are shown in Figures 10 and 11, and likewise for the RCP8.5 greenhouse gas concentration pathway in Figure 12 to Figure 15.

[c] The maximum RX1day over the 30-year analysis period is selected to focus the analysis on extreme rainfall. We note that different results may arise over shorter analysis periods, or if the mean value over the analysis period were selected instead.

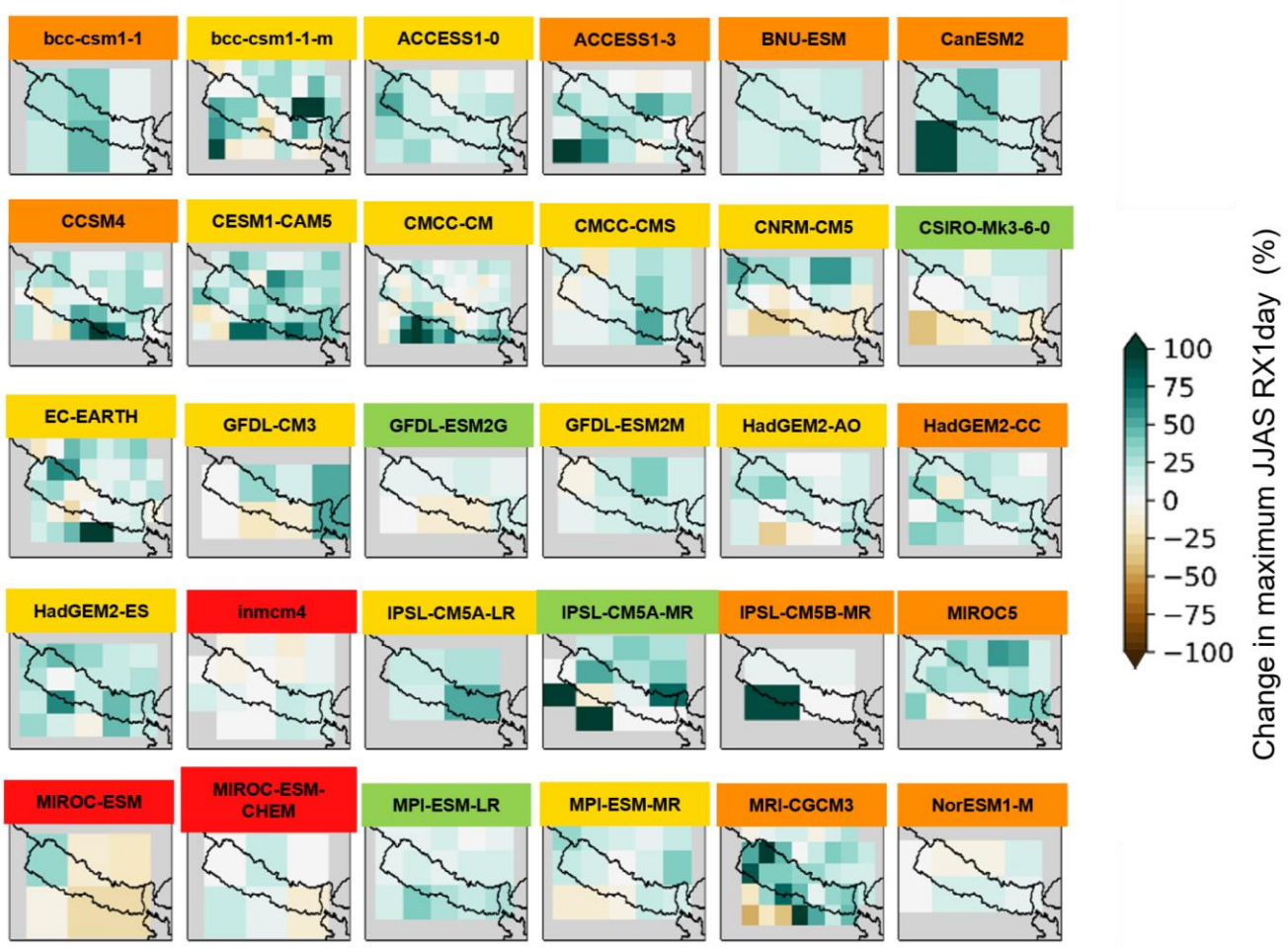

Figure 8 Maps of projected change in maximum JJAS RX1day for the 2050s under RCP4.5 for 30 CMIP5 GCM simulations. The colour of the model name represents the evaluation category from the assessment in Richardson (2021).

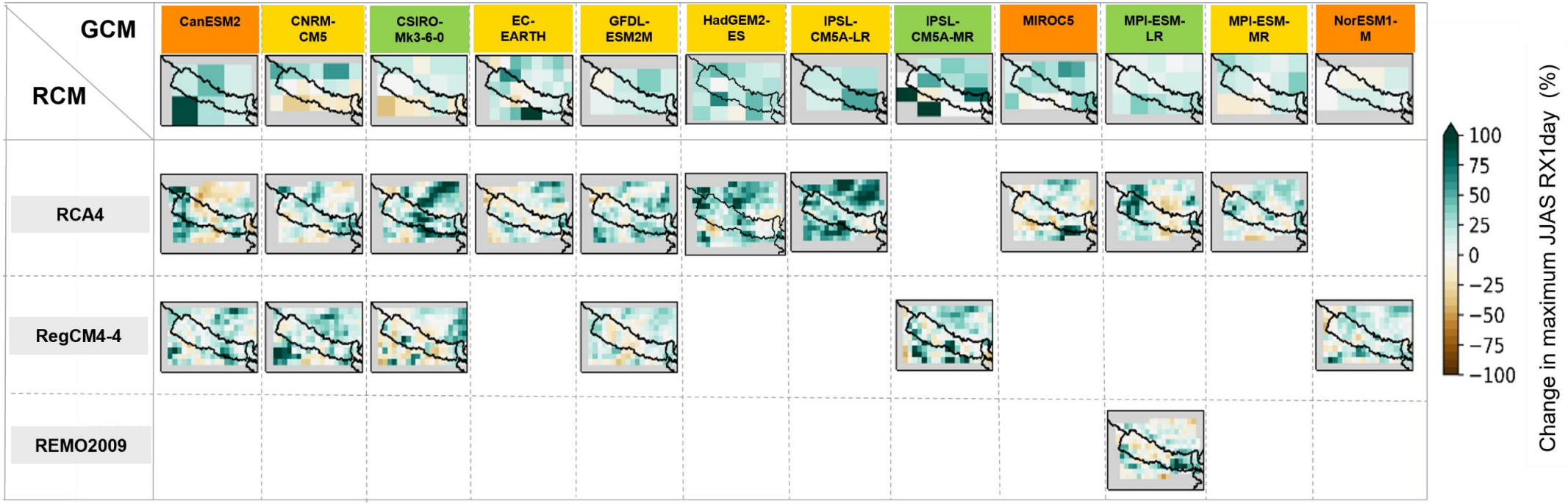

Figure 9 Maps of projected change in maximum JJAS RX1day for the 2050s under RCP4.5 for the 17 RCM simulations from CORDEX WAS-44. Projected changes from the driving GCM simulations are also included, and the 17 RCM projections are arranged by their driving GCM (columns) and the RCM used (rows). The colour of the driving GCM model name represents the evaluation category from the assessment in Richardson (2021).

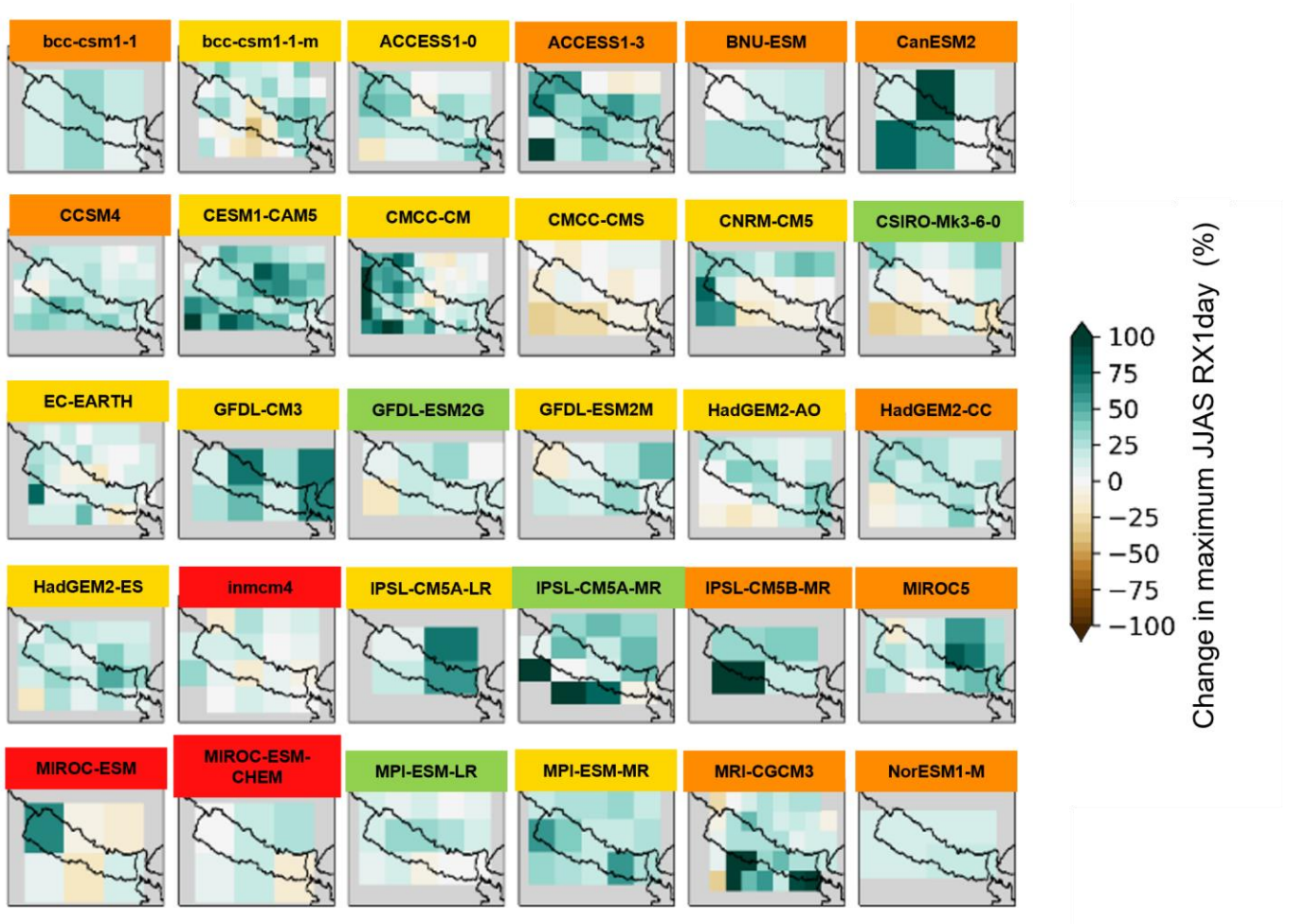

Figure 10 Maps of projected change in maximum JJAS RX1day for the 2080s under RCP4.5 for 30 CMIP5 GCM simulations. The colour of the model name represents the evaluation category from the assessment in Richardson (2021).

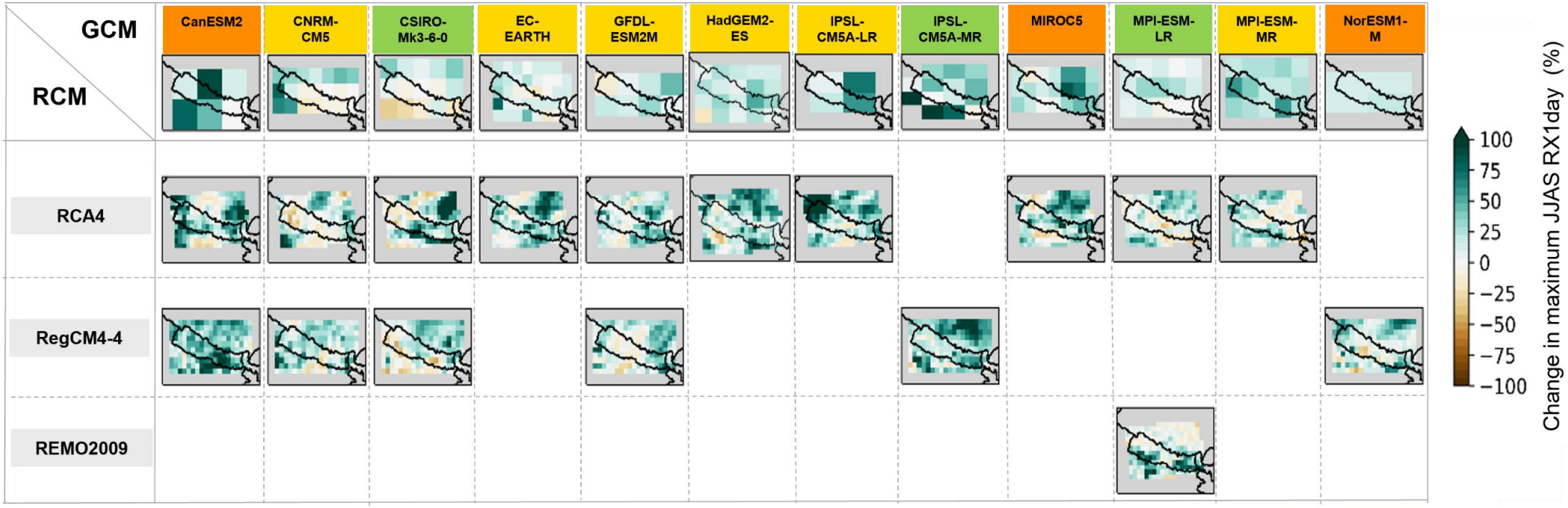

Figure 11 Maps of projected change in maximum JJAS RX1day for the 2080s under RCP4.5 for the 17 RCM simulations from CORDEX WAS-44. Projected changes from the driving GCM simulations are also included, and the 17 RCM projections are arranged by their driving GCM (columns) and the RCM used (rows). The colour of the driving GCM model name represents the evaluation category from the assessment in Richardson (2021).

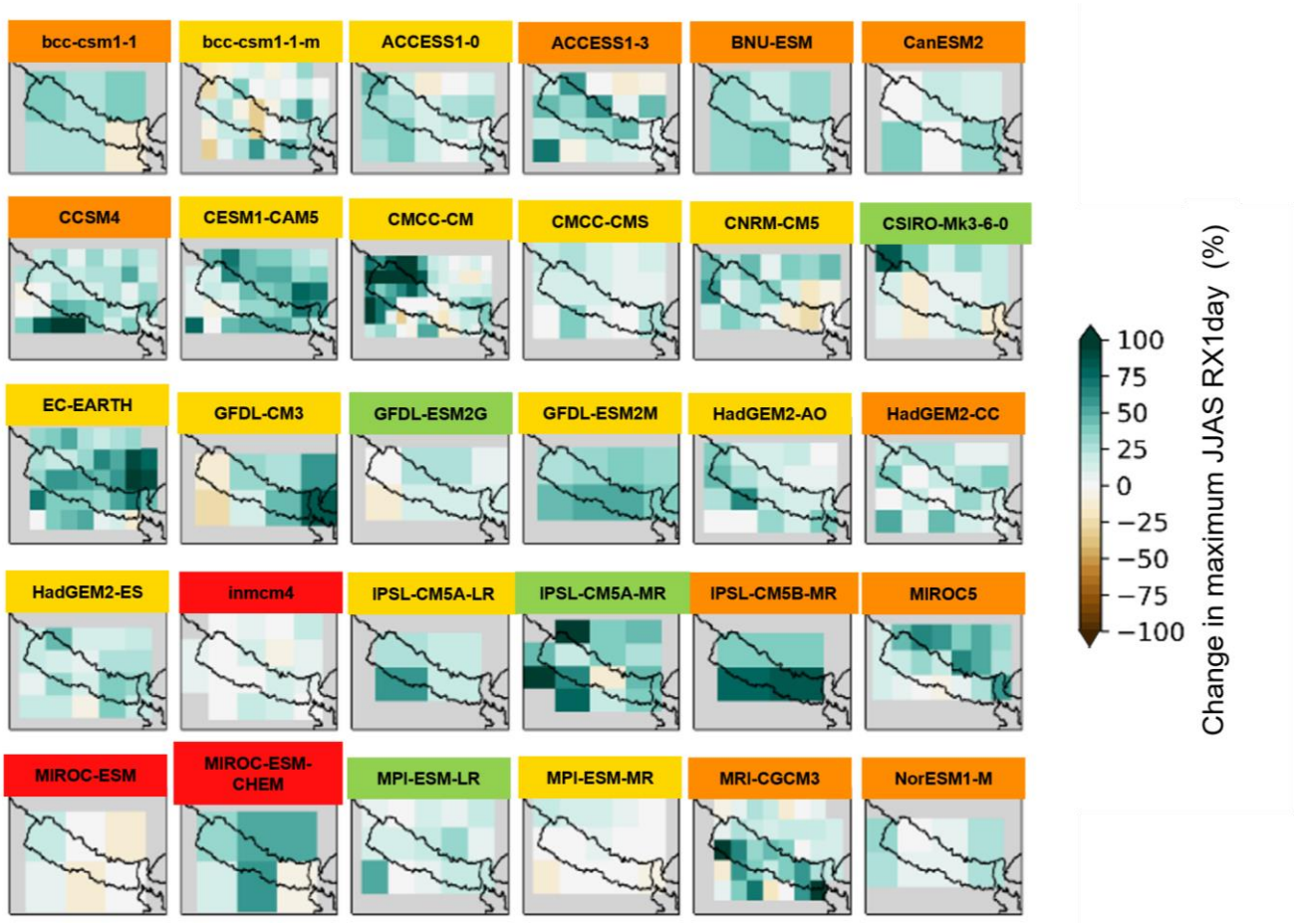

Figure 12 Maps of projected change in maximum JJAS RX1day for the 2050s under RCP8.5 for 30 CMIP5 GCM simulations. The colour of the model name represents the evaluation category from the assessment in Richardson (2021).

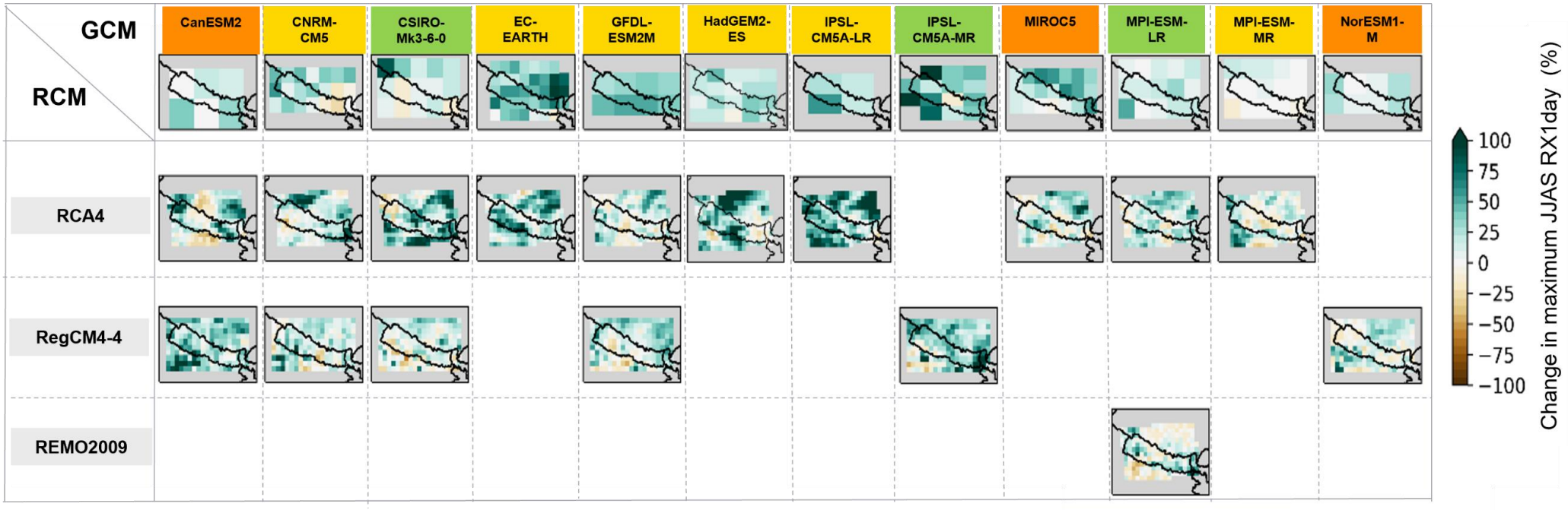

Figure 13 Maps of projected change in maximum JJAS RX1day for the 2050s under RCP8.5 for the 17 RCM simulations from CORDEX WAS-44. Projected changes from the driving GCM simulations are also included, and the 17 RCM projections are arranged by their driving GCM (columns) and the RCM used (rows). The colour of the driving GCM model name represents the evaluation category from the assessment in Richardson (2021).

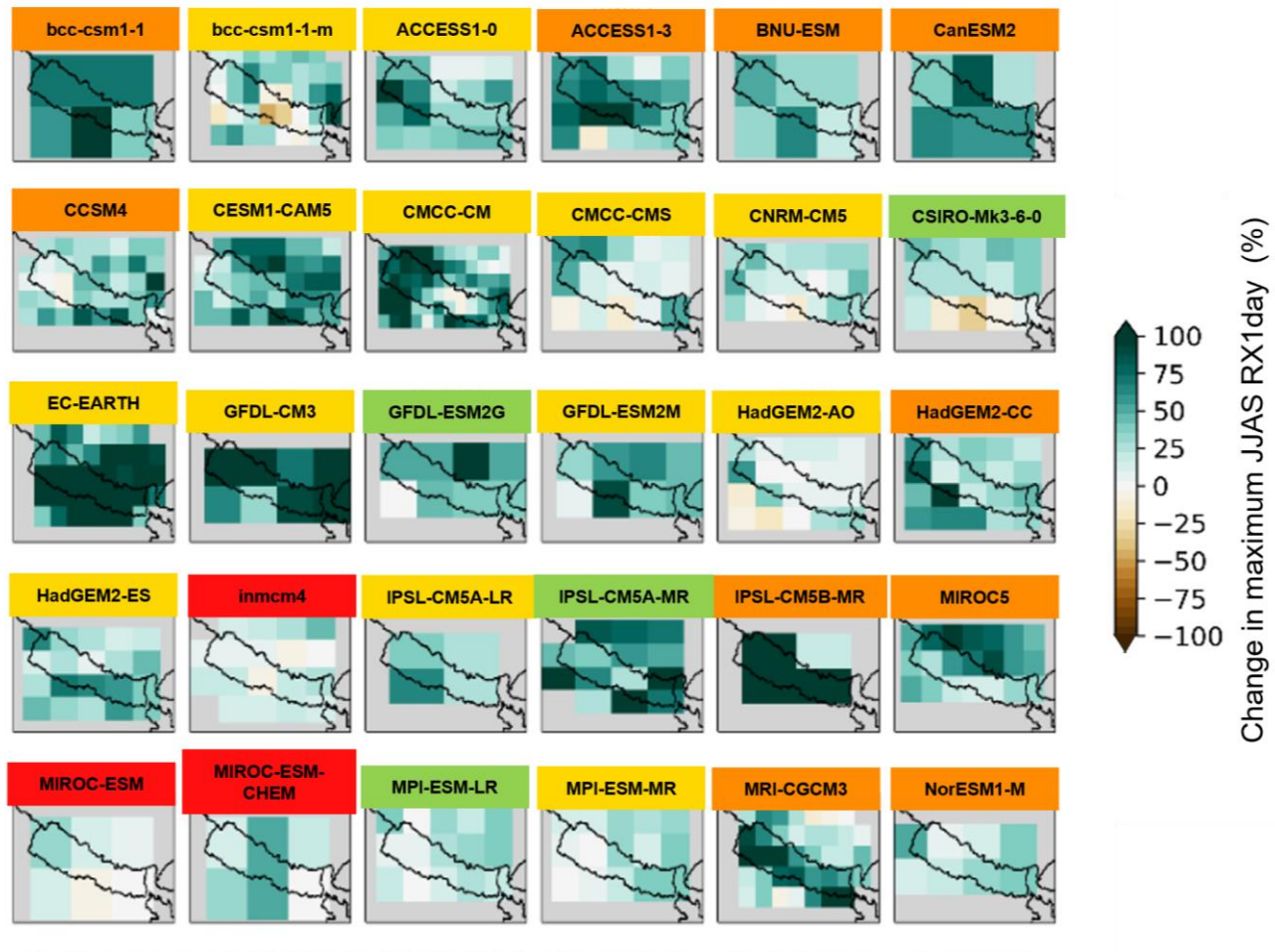

Figure 14 Maps of projected change in maximum JJAS RX1day for the 2080s under RCP8.5 for 30 CMIP5 GCM simulations. The colour of the model name represents the evaluation category from the assessment in Richardson (2021).

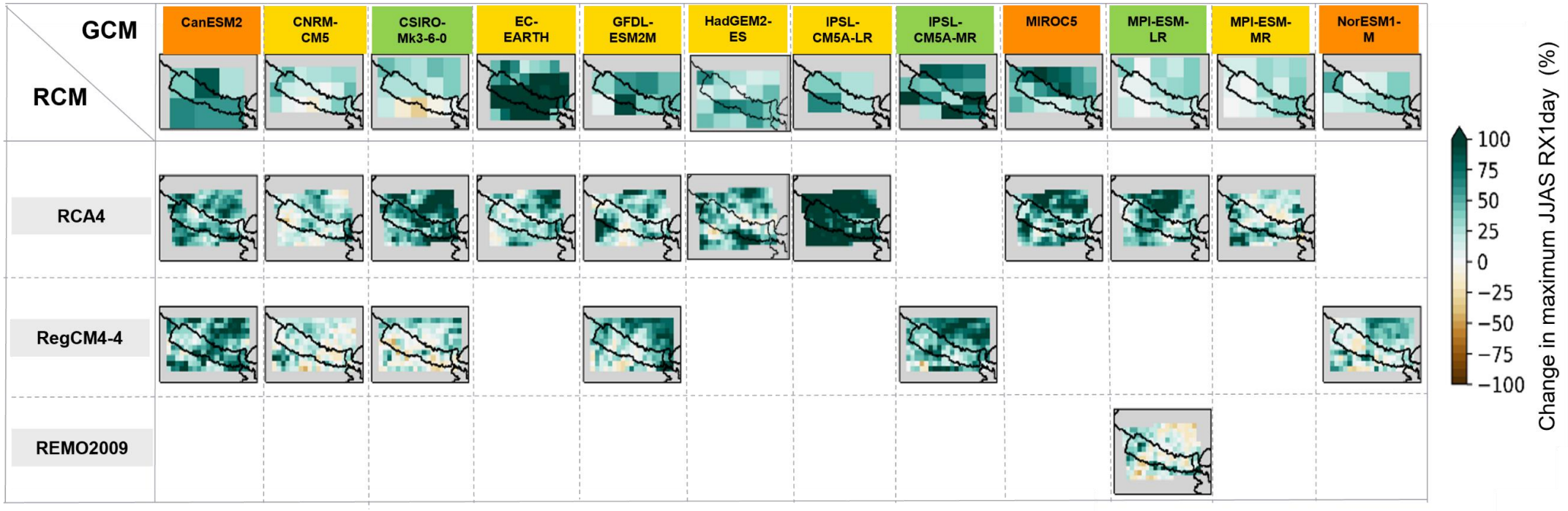

Figure 15 Maps of projected change in maximum JJAS RX1day for the 2080s under RCP8.5 for the 17 RCM simulations from CORDEX WAS-44. Projected changes from the driving GCM simulations are also included, and the 17 RCM projections are arranged by their driving GCM (columns) and the RCM used to downscale that projection (rows). The colour of the driving GCM model name represents the evaluation category from the assessment in Richardson (2021).

The maps show a general increase in maximum RX1day in the future climate, with larger increases in general under the RCP8.5 greenhouse gas concentration scenario and for the 2080s. However, there is large spatial variability across Nepal in most of the model projections, with many showing both increases and decreases across the region, and there is no consistent pattern of change across the model projections. Under the RCP8.5 scenario in the 2080s (e.g., Figure 14 and Figure 15), there is a more consistent increase across the model projections but the magnitude of increases still varies widely, with some showing very large increases and some showing little change.

Furthermore, these maps also show that the RCM simulations create very different internal climates that are largely unconstrained from the driving GCM (e.g. compare projected changes from the GCM with the RCM downscalings in Figures 9, 11, 13 and 15). This emphasizes the large natural variability and model dependence associated with extreme precipitation. This also justifies the focus of our analysis on dynamically downscaled projections that can better simulate these processes over statistical downscaling techniques.

Although there is large spatial variability in the projected changes of maximum JJAS RX1day across Nepal, a spatial mean of the data is useful to calculate Nepal-average values and compare changes from across the model projections[d]. Figure 15 and Figure 16 show the spread of projected changes in maximum JJAS RX1day across all model simulations considered for the 2050s in the RCP4.5 and RCP8.5 pathways respectively. The specific values from these boxplots are presented in Appendix D.

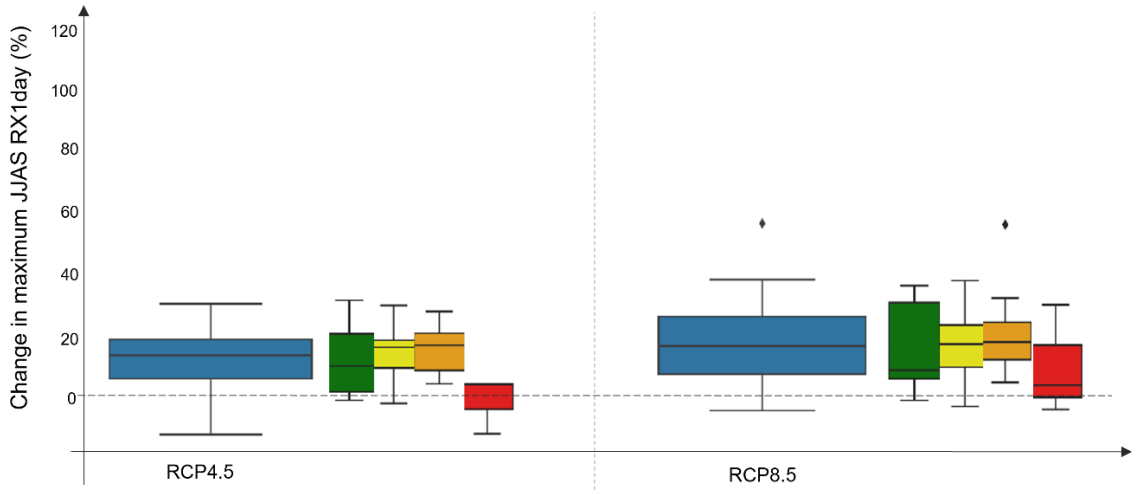

Figure 16 Boxplots of the projected change in JJAS maximum RX1day for the 2050s under RCP4.5 (left panel) and RCP8.5 (right panel) from all 30 CMIP5 and 17 CORDEX WAS-44 model simulations. Blue boxplots show the results from the full ensemble of model simulations considered. The equivalent boxplots filtered by GCM assessment category are included for each RCP to demonstrate how the different GCMs contribute to the full spread of values.

[d] A spatial mean is taken across a box of data around Nepal, as presented in Figure 8 to Figure 15, rather than extracting the values for the country shape to enable effective comparison between the CORDEX and CMIP5 data. This accounts for the low resolution of the CMIP5 models.

The blue boxplots (left-most boxplots) show that the majority of model projections show an increase in the spatially averaged maximum JJAS RX1day for both RCPs, but some model projections show a decrease. The smaller boxplots, to the right of the blue boxplots, show the spread of values from the green (well-performing), yellow and orange (use with caution), and red (poor-performing) categorised GCMs; the RCM model simulations are categorised by their driving GCM. This breakdown by GCM category shows that:

- For RCP4.5 in the 2050s, the larger negative values come from the red categorised GCM simulations, which gives justification for discounting these values from the range of plausible values.

- Across both RCPs in the 2050s, the green and yellow categorised GCM simulations span the majority of the full range of values (excluding the larger negative values in RCP4.5), giving justification for values represented by the upper tails of the boxplots, and the lower end of the range of values being close to zero.

- The model projection identified as an outlier of the distribution (black dot for RCP8.5) comes from a model projection where the GCM is in the orange category meaning that it failed on some of the assessment metrics and should be used with caution.

Similar boxplots for projected changes in maximum JJAS RX1day in the 2080s under both RCP4.5 and RCP8.5 are shown in Figure 17. The specific values from these boxplots are presented in Appendix D. These boxplots show:

- A larger spread in values compared to those for the 2050s, particularly under RCP8.5.

- The red categorised GCM simulations that should be excluded generally represent small increases, so are not representative of the full range of model projections.

- For RCP4.5 in the 2080s there are some model simulations that project a decrease in maximum JJAS RX1day. The largest of these comes from a yellow categorised GCM simulation which has not had a full evaluation assessment and has relatively low resolution. One CORDEX model simulation that was driven by a green categorised GCM simulation projects a small decrease. There are no negative projections under RCP8.5, but some green categorised GCM simulations project very small increases. This again justifies the exclusion of large negative changes but the inclusion of a future scenario where there is little change compared to the present day.

- The green categorised GCM simulations generally span the full range of projections for both RCPs, including the largest values for RCP8.5 which are classified as outliers of the full distribution. This gives justification for including a scenario that accounts for these very large increases, but with lower confidence.

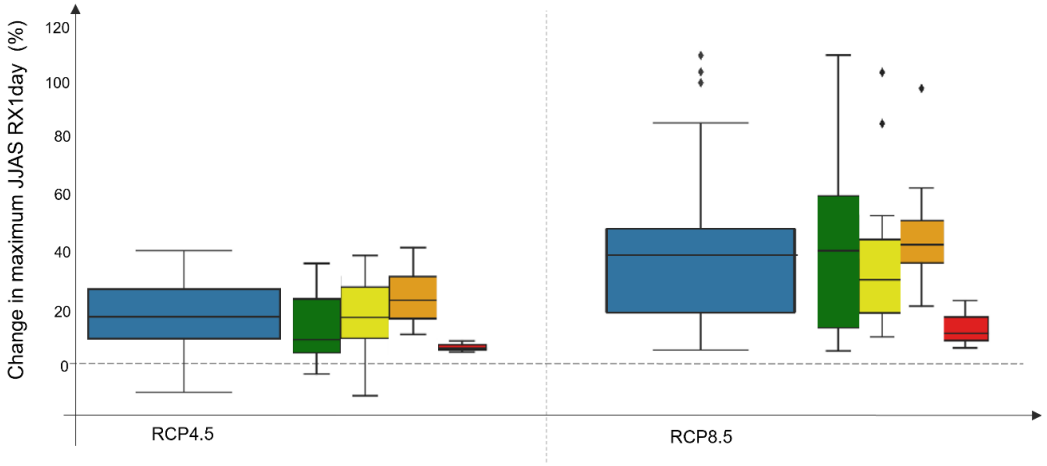

Figure 17 Boxplots of the projected change in JJAS maximum RX1day for the 2080s under RCP4.5 (left panel) and RCP8.5 (right panel) from all 30 CMIP5 and 17 CORDEX WAS-44 model simulations. Blue boxplots show the results from the full ensemble of model simulations considered. The equivalent boxplots filtered by GCM assessment category are included for each RCP to demonstrate how the different GCMs contribute to the full spread of values.

3.2 Selecting a subset of models that represent the range of plausible changes

A subset of model simulations that span the range of plausible projections in maximum JJAS RX1day for the two RCP pathways were selected. The criteria for selection included:

- Prioritise RCM simulations,
- model simulations that represent the range of projections across the RCPs and future time periods,
- a preference for driving GCMs in the green category, as these model simulations best represent the processes that drive extreme precipitation in the region,
- a preference to span all three RCMs in the CORDEX WAS-44, and a unique selection of GCM-RCM couplings to span the range of available options.

The specific model simulations in each of the scenario selection categories are presented in Table 1 and the ordered values that were used to identify these models are included in Appendix C. Projected changes in maximum JJAS RX1day from this subset of model simulations per RCP are plotted together in Figure 18 and the associated maps from these model simulations are shown in Figure 19.

Table 1 Model simulations selected for the subset that spans the range of plausible changes.

Scenario selection category	RCP	Model simulation selected	
		RCM	GCM
Model simulations representing the lower end of projected changes – the lowest change.	RCP4.5	RegCM4-4	CSIRO-Mk3-6-0
	RCP8.5	RegCM4-4	CSIRO-Mk3-6-0
Model simulations representing the upper end of projected changes – the largest change and often outliers of the distribution.	RCP4.5	RegCM4-4	CanESM2
	RCP8.5	RCA4	IPSL-CM5A-MR
Model simulations representing the second largest projected changes which are more representative of the upper quartile of model projections.	RCP4.5	RCA4	IPSL-CM5A-MR
	RCP8.5	RCA4	CSIRO-Mk3-6-0
Model simulations representing the middle of the range of projected changes	RCP4.5	REMO2009	MPI-ESM-LR
	RCP8.5	RCA4	MPI-ESM-LR

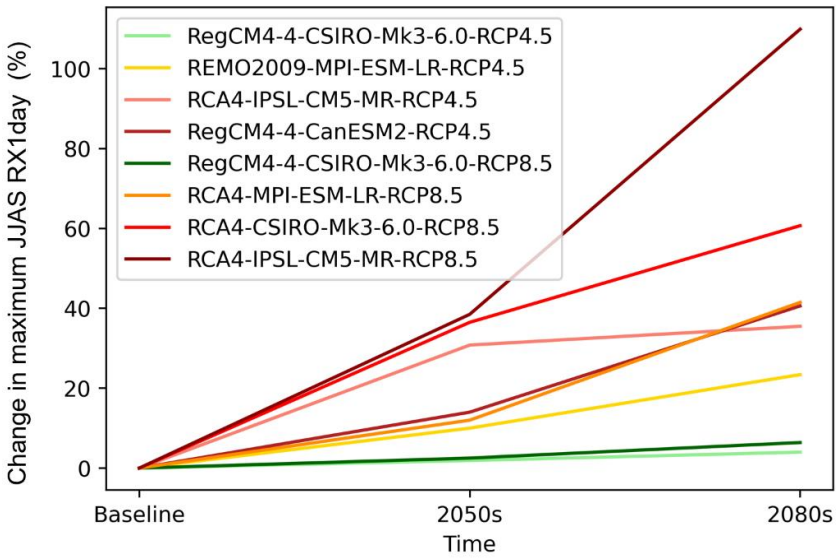

Figure 18 Changes in maximum JJAS RX1day for the 2050s and 2080s for the subset of CORDEX model simulations that span the range of plausible projections. The corresponding maps are shown in Figure 19.

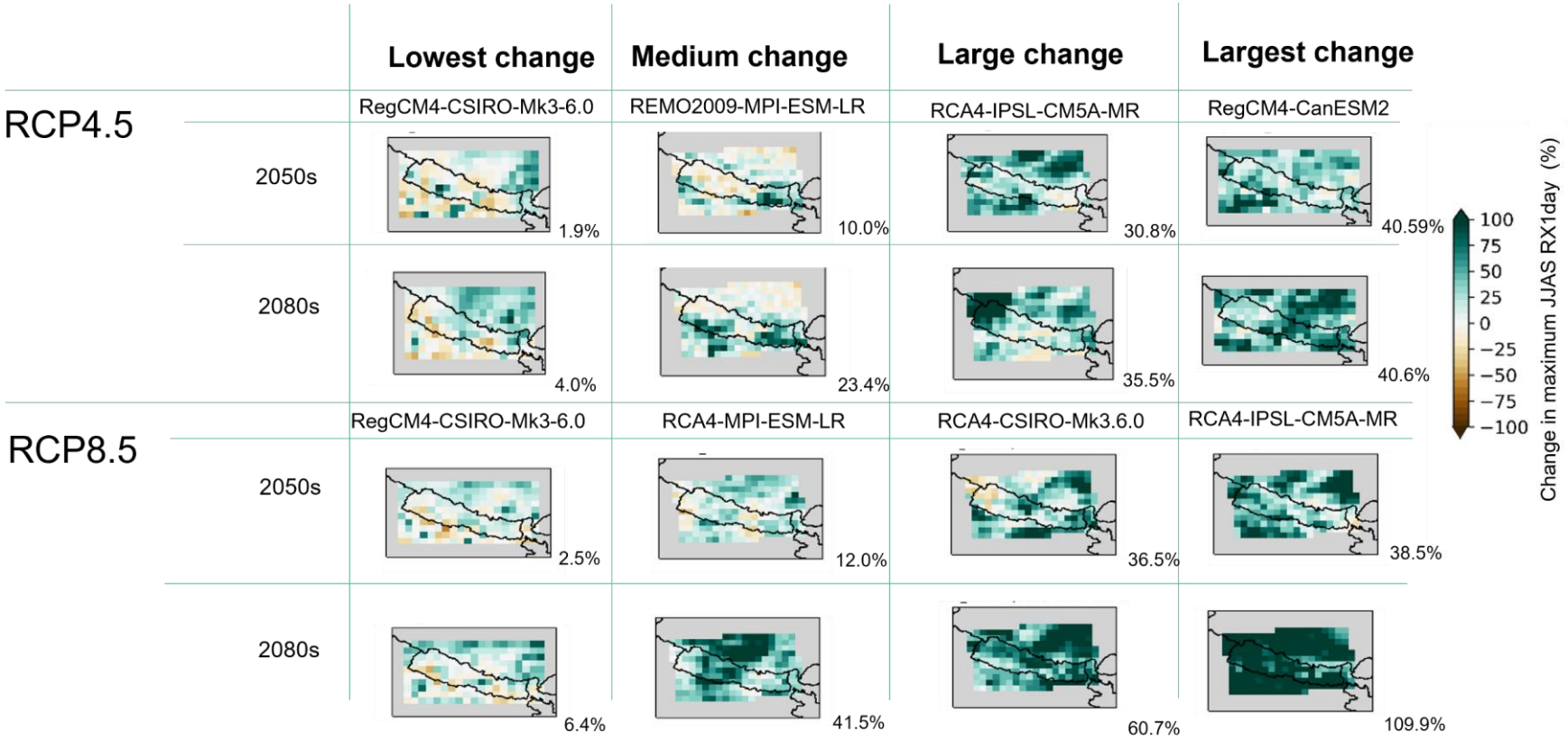

Figure 19 Selected maps of representative projected changes of JJAS RX1day from the model subset. The numbers in the bottom right of each map panel show the spatial mean.

3.2.1 *A set of representative scenario pathways of changes in extreme monsoon precipitation in Nepal*

Results from this subset of model simulations were distilled into four plausible scenarios of changing maximum JJAS RX1day through the 21st century following the climate information distillation process presented in Daron et al. (2022). The four scenarios are plotted in Figure 20 and descriptions given below:

- 'Little change' scenario: little change in maximum JJAS RX1day in both the 2050s and 2080s; taken from the RegCM4-4-CSIRO-Mk3-6-0 model simulation.
- 'Moderate increases' scenario: an increase in maximum JJAS RX1day of 15% by the 2050s and 30% in by the 2080s, relative to the baseline climate; represents results from the middle of the range of projections.
- 'Large increases' scenario: an increase in JJAS RX1day of 35% by the 2050s and 60% in the 2080s, relative to the baseline climate; the upper quartile of the range of projections.
- 'Very large increases' scenario: an increase in JJAS RX1day of 40% by the 2050s and 110% by the 2080s, relative to the baseline climate; represents the high end of the range of projections.

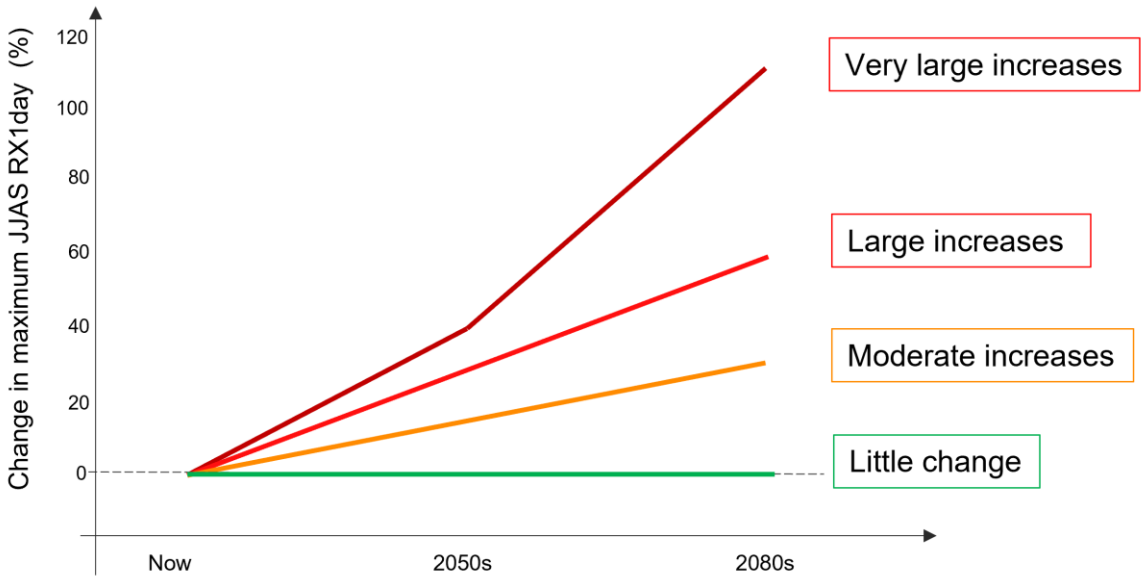

Figure 20 Four plausible scenarios of future changes in daily maximum precipitation during the monsoon season in Nepal, spanning the range of model projections.

3.3 Best estimate of CORDEX future changes

The CORDEX model simulations, presented in Section 3.1, can be further used to develop estimate absolute RX1day values, by applying a change factor approach (e.g. Anandhi et al., 2011) to the best observational data produced in Section 2.

For this approach, a future RX1day estimate $RX1day_{FUT}$ is calculated as:

$$RX1day_{FUT} = RX1day_{HIST} \times \left(\frac{RCM_{FUT}}{RCM_{HIST}} \right) \quad (10)$$

Where RCM_{FUT} and RCM_{HIST} are future RX1day estimates from selected CORDEX model simulations for RCP4.5 or RCP8.5 scenarios, and $RX1day_{HIST}$ are the GAM estimates presented in Section 2. By further applying the GAM methodology used to produce $RX1day_{HIST}$ (Section 2.1) to the CORDEX model simulations, we produce a best estimate of CORDEX RX1day that are spatially and temporally consistent. The formulation is almost identical to Equations (1) – (4), except we now have group level effects u_m for $m = 1 \ldots 17$ CORDEX model simulations with driving GCMs that are classified as being green or yellow (see Figure 15). CORDEX model simulations with driving GCMs classified as red or orange are excluded. Two separate statistical models are fitted for each RCP scenario, for future periods equal to 2050 and 2080. As for Section 2, RCM_{FUT} and RCM_{HIST} estimates are done on a 0.35° x 0.23° grid and based on JJAS block-maxima

We summarise the change factors in Table 2. Although we calculate change factors at each grid box, the spatial variability is small (not shown) and we choose to summarise change factors as a Nepal mean value. Table 2 shows that changes to smaller magnitude, more frequent RX1day extremes are likely to be greater (+40% for a 1-in-2 year event under RCP8.5 by 2080) than changes to larger magnitude, less frequent RX1day extremes (+21% for a 1-in-100 year event under RCP8.5 by 2080). A full breakdown of projected changes for each model simulation are shown in Appendix D. Figure 21 and Figure 22 show the changes factors from Table 2 applied to the observational estimates of Figure 2.

Table 2 Summary of JJAS RX1day change factors based on a subset of CORDEX model simulations with green or yellow diving GCMs. Projected changes represent the 50th percentile Nepal-mean value for RCP4.5 and RCP8.5 scenarios in 2050 and 2080 for 4 different return periods, from extreme value analysis of JJAS block-maxima. Change factors are rounded to the nearest percent.

Return Period (years)	RCP	2050	2080
2	RCP4.5	12%	21%
	RCP8.5	19%	40%
20	RCP4.5	7%	12%
	RCP8.5	11%	24%
100	RCP4.5	6%	11%
	RCP8.5	10%	22%
200	RCP4.5	6%	10%
	RCP8.5	9%	21%

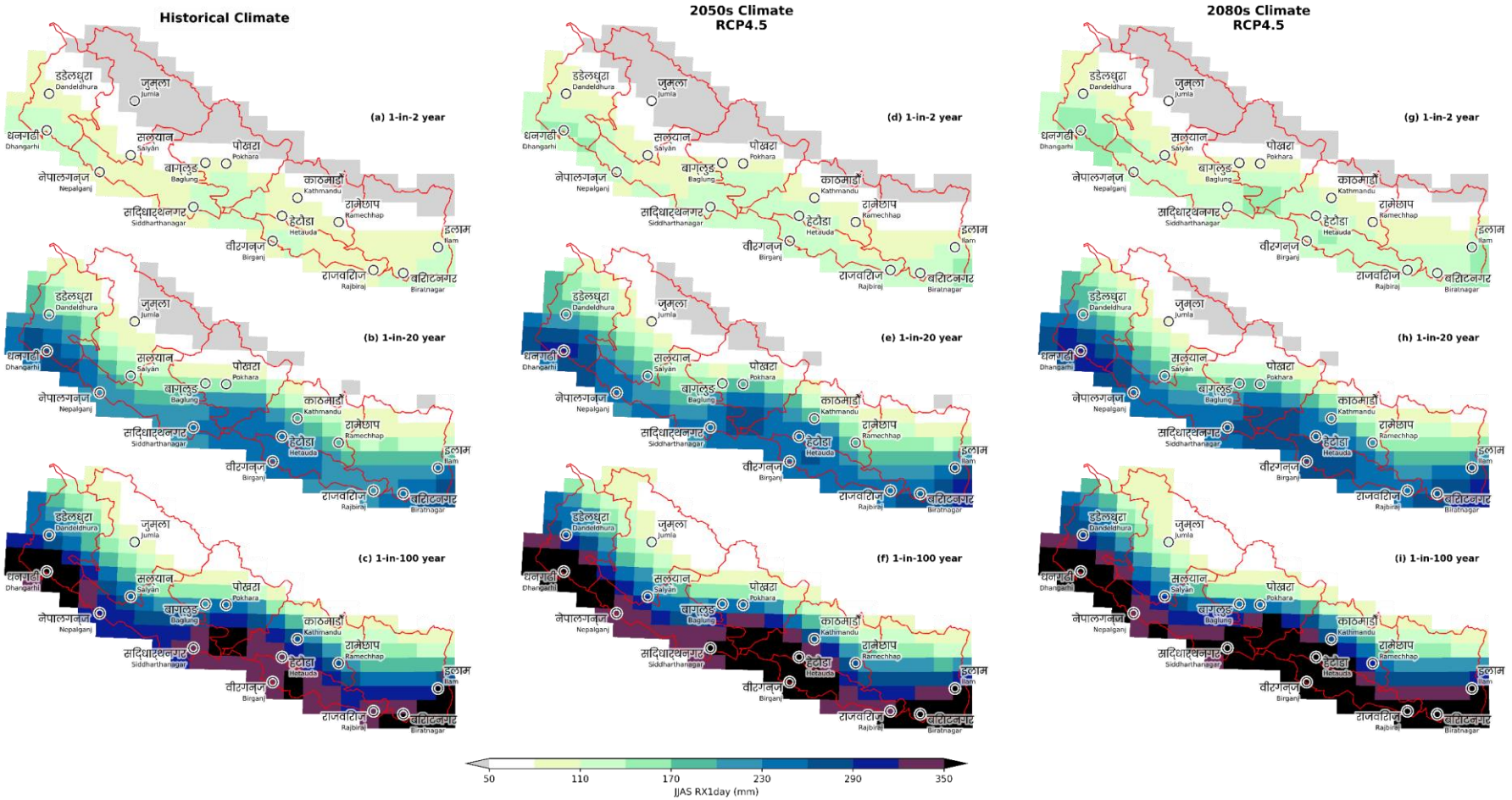

Figure 21 Return period estimates for JJAS RX1day comparing the historical climate (a-c) with median changes under RCP4.5 for 2050 (c-f) and 2080 (g-i).

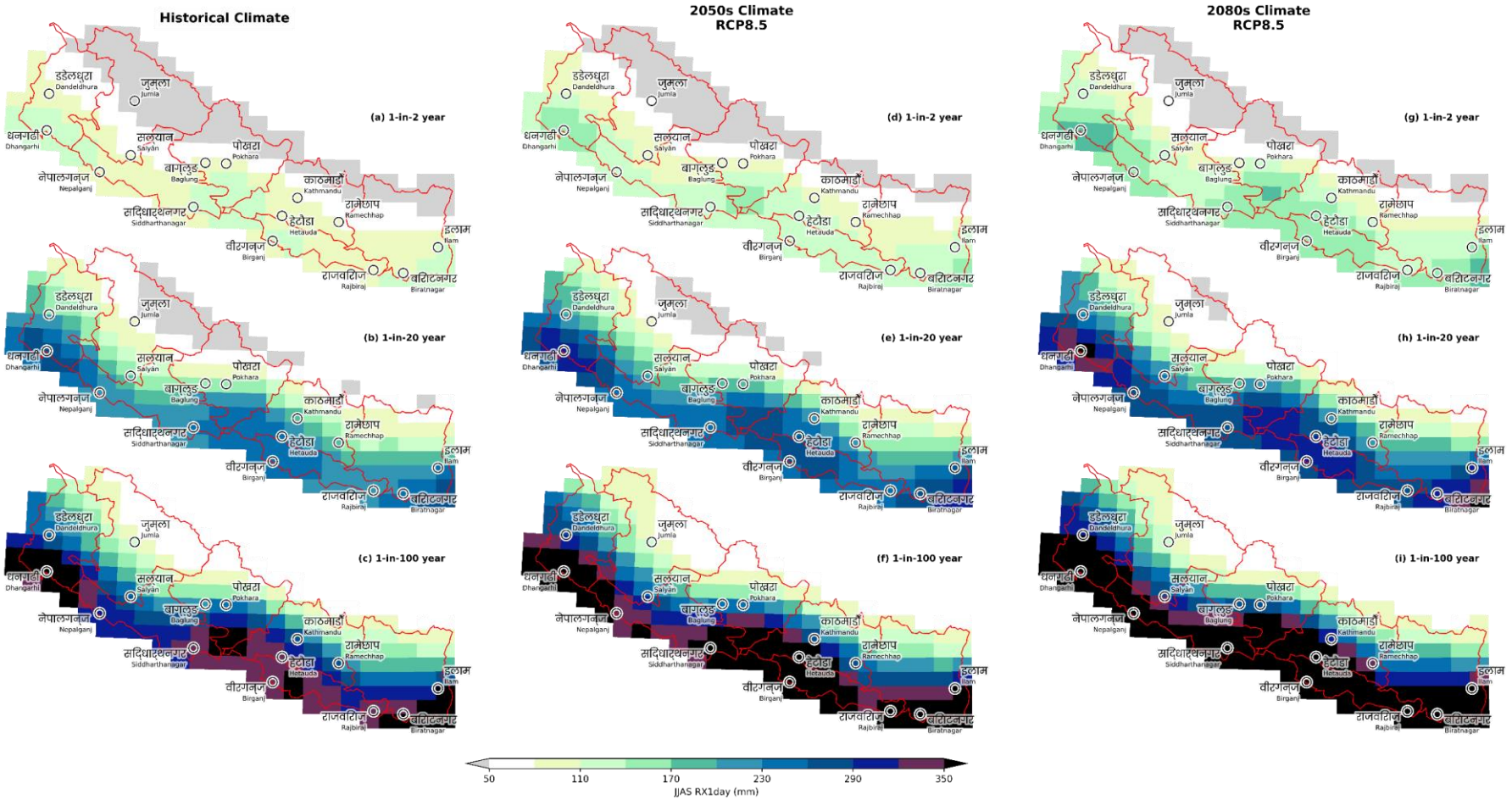

Figure 22 Return period estimates for JJAS RX1day comparing the historical climate (a-c) with median changes under RCP8.5 for 2050 (c-f) and 2080 (g-i).

4. Summary & Conclusions

This report forms the culmination of a series of reports on understanding and quantifying extreme precipitation events in South Asia. It draws on the outputs of Parts I-III in the report series and focuses on quantifying the risk of extreme monsoon precipitation in Nepal to support engagement with stakeholders and planners in the hydropower sector in Nepal.

We take a two-part approach to assess current and future changes to extreme 1-day precipitation accumulation (RX1day) in Nepal. For the current climate, we build a blended dataset based on selected observational datasets (MSWEP v2.8, HAR v2, IMDAA and GloSea5) that contribute the best information over Nepal's complex topography. We highlight that (in terms of precipitation averaged over ~800 km2):

- The chance of high RX1day accumulations is generally greater in our blended datasets than in ERA5 or Aphrodite-2 alone.
- Large parts of the Terai and Hill regions have the potential to see RX1day accumulations of 140 mm at least every 2 – 5 years.
- Some parts of the Terai could receive one-day precipitation accumulations in excess of 350 mm once every 100 years.

For the future climate, we build on our previous process-based evaluation to distil available climate model simulations into a set of four plausible scenarios of projected changes in maximum JJAS RX1day. We find that:

- There is large spatial variability in the projected changes in maximum JJAS RX1day across Nepal.
- The majority of model projections show an increase in maximum JJAS RX1day when averaged across Nepal, however there is a large spread in the magnitude of change.
- The four scenarios identified that span the range of plausible projections range from little change in maximum JJAS RX1day by the end of the century to increases of over 100%.

We also estimated the most likely range for the changes in RX1day precipitation accumulation under RCP4.5 and RCP8.5 greenhouse gas concentration scenarios and find that:

- Under RCP4.5 (by the end of the century) our best estimate for RX1day change is 10 – 21%. Under RCP8.5 it is 21 – 40%.
- Changes to more frequent low-threshold RX1day extremes are likely to be greater than changes to high-threshold less frequent RX1day extremes.

4.1 Limitations and future work

For our analysis of present day extremes, a key limitation was the unavailability of comprehensive rain gauge data from DHM. Although Aphrodite-2 and IMDAA datasets include some Nepal rain gauge data, we are anecdotally aware that these datasets do not include the full breadth of data collected by DHM. Future work should seek to include this data. For the purposes of hydrological modelling, our analysis is not temporally consistent at the scale of hydrological basins. An adaptation of the HGAM fitting, working at basin scales, rather than grid-box scale could be a useful extension for the purposes of event-based hydrological modelling.

For future extremes, we recognise that the RCP4.5 and RCP8.5 greenhouse gas concentration scenarios are a limited sample of potential future changes. Future changes in greenhouse gas concentrations could reasonably be both higher or lower than either of these scenarios. Future work could include inclusion of higher resolution RCM simulations from the CORDEX CORE experiments, as well as CMIP6 GCM projections and any future regional downscalings of CMIP6 model simulations.

4.2 Recommendations for the hydropower sector in Nepal

The assessments of the risk of extreme monsoon precipitation both in the current climate and under a changing climate presented here can be used to inform long-term planning for the hydropower sector in Nepal.

Improved understanding of the risk of extreme monsoon precipitation in the current climate can be used to inform improvements to the climate resilience of existing hydropower projects and operations. We have demonstrated that individual observational data products do not give accurate assessments of extreme precipitation events and that these estimates are less likely to be underestimated by combining multiple sources of data. We therefore recommend the use of multiple sources of data for quantifying precipitation return periods for an improved assessment of present-day risk. Ideally, these data sources should derive from several different collection methods, to avoid specific limitations inherent to them individually.

This improved understanding of current risks can also help to inform the development and design of future hydropower plants, alongside the information provided here about how these risks may change in the future climate. The four plausible scenarios of projected changes in extreme monsoon precipitation, can be used to explore possible futures the hydropower sector will need to prepare for, ranging from little change relative to the current climate to a potential doubling in the magnitude of RX1day. This could be done in a qualitative manner in collaboration with stakeholders to explore what the different scenarios of projected changes might mean, such as through the use of Climate Risk Narratives[e]. Additionally, the scenarios can be used in a quantitative way to explore how the projected changes in

[e] The scenarios were used to inform an interactive session on Climate Risk Narratives for Nepal at a workshop in July 2022, the outputs are available on the CARISSA website

precipitation translate into river flow and other variable relevant to the hydropower sector, through further collaboration with scientists and stakeholders in Nepal.

Appendix A. Data & Code Availability

Data used in the analysis of present-day extremes is available as follows:

- **MSWEP v2.8:** (Beck et al., 2019) Openly accessible (CC BY-NC 4.0) from http://www.gloh2o.org/mswep/
- **HAR v2**: (Wang et al., 2021) Openly accessible from https://www.klima.tu-berlin.de/index.php?show=daten_har2
- **IMDAA:** (Rani et al., 2021) Openly accessible from https://rds.ncmrwf.gov.in/datasets
- **GloSea5 N512**: (Scaife et al., 2019) Not openly accessible. Please contact the authors for data requests.

Data use in the analysis of future extremes comes from openly accessible CORDEX South Asia domain. Details on accessing CORDEX data are available at https://cordex.org/data-access/.

Data analysis in this report makes use of mgcv in R (available from https://cran.r-project.org/web/packages/mgcv/index.html) and Iris in Python (available from https://github.com/SciTools/iris).

Appendix B. Statistical Model Evaluation Plots

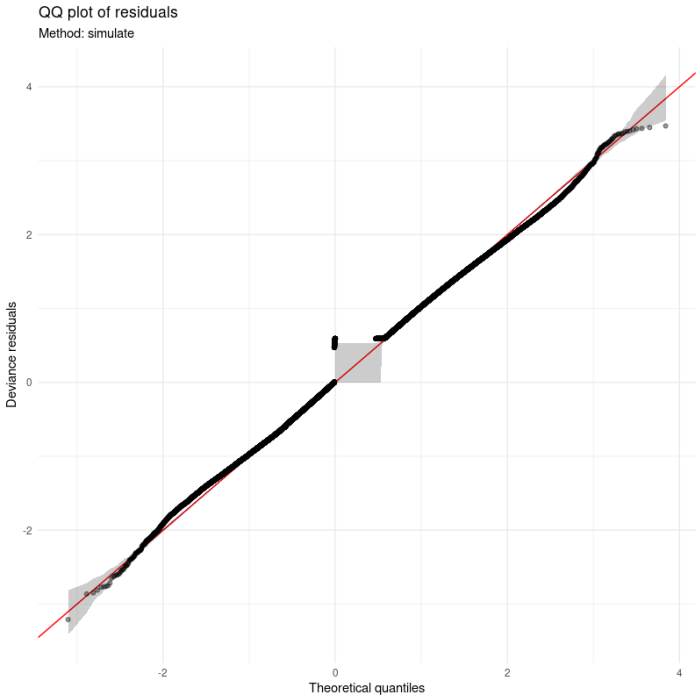

Figure 23 Quantile-quantile plot of model residuals, with 90% reference interval (grey shading) based on 50 simulations of the GAM specified in Equation 1.

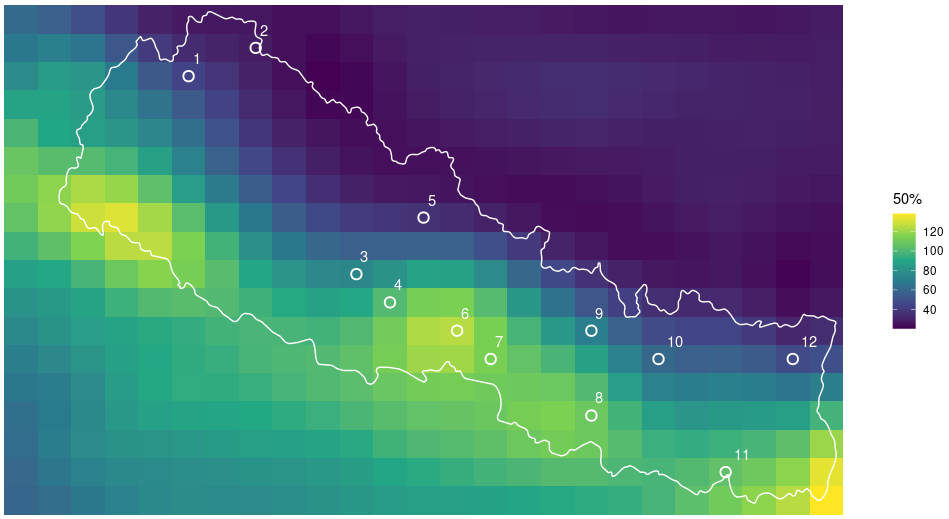

Figure 24 Evaluation locations for 12 randomised points in Nepal, used to compare GAM model fit with input data, shown in Figure 25. Background shading is the median 1-in-2 year RX1day estimate as in Figure 2.

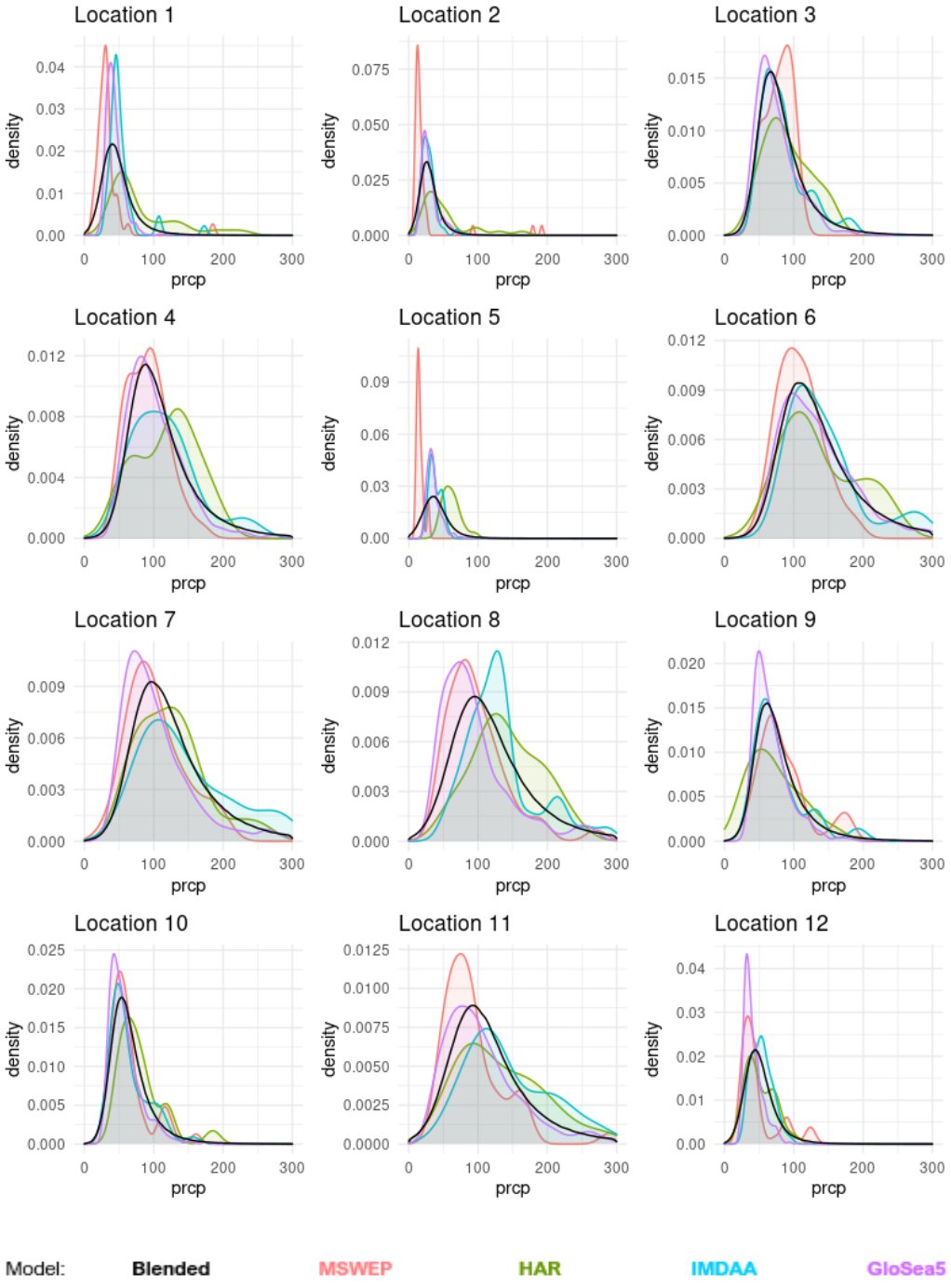

Figure 25 Kernel density estimations of observed datasets (coloured) comparison to the simulated GAM model distribution (black), for the 12 random locations as specified in Figure 24. X-axis values are grid area-averaged RX1day in mm.

Appendix C. Process-based evaluation flow diagram

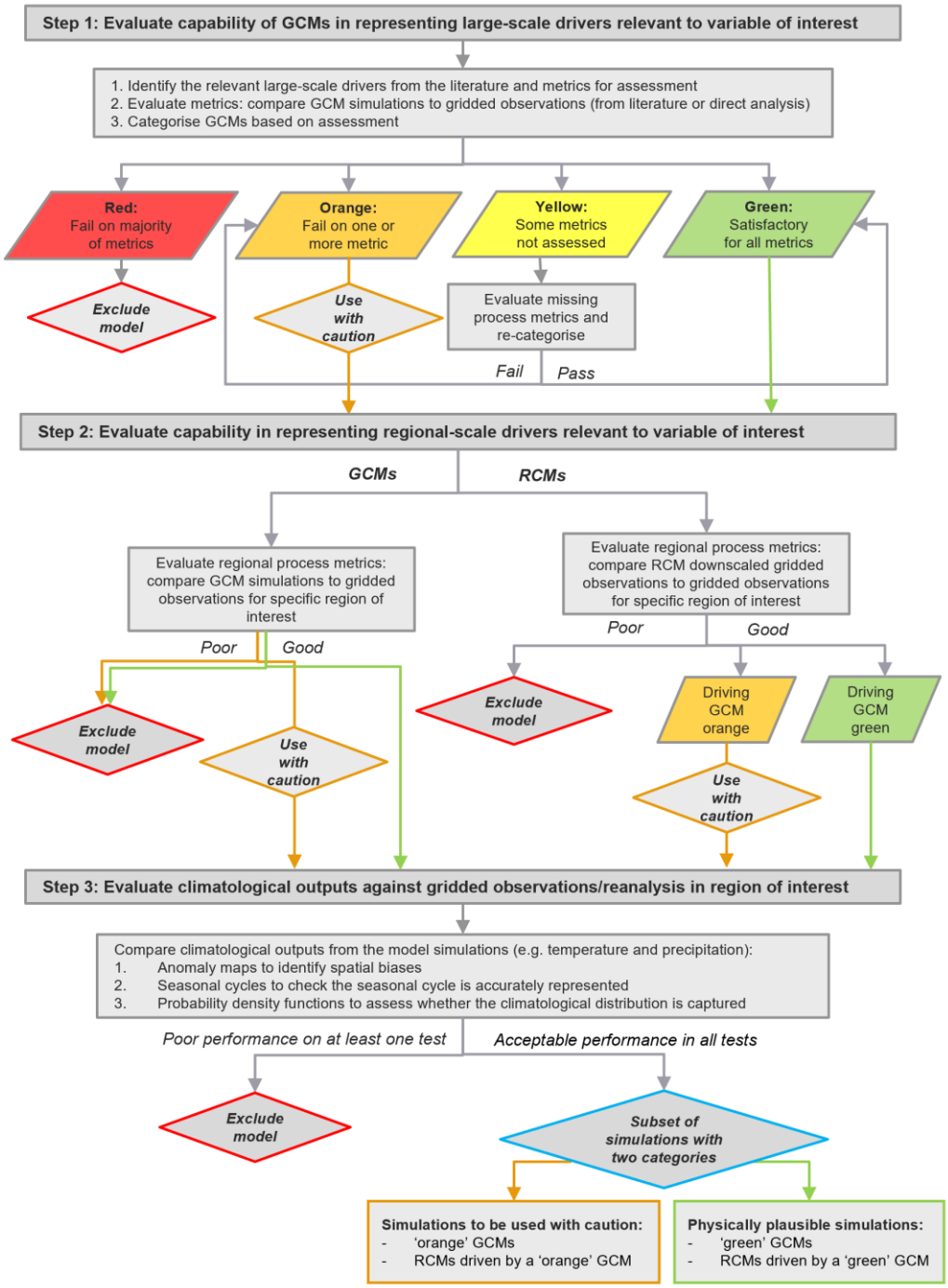

Figure 26: Schematic of best practice in a process-based evaluation process. Step 1 was conducted in Richardson (2021) to assess the capability of the CMIP5 GCMs.

Appendix D. Tables of projected changes in RX1day

Table 3: Values of the projected change in JJAS maximum RX1day averaged over Nepal under RCP4.5. The data is sorted based on the value of the projected change in the 2080s. CMIP5 GCM names are coloured based on their assessment category from Richardson (2021) and the RCM used to generate the regionally downscaled projections from CORDEX are included in the RCM column or left blank if a GCM projection.

GCM	RCM	Change in Rx1day (%) 2050s	Change in Rx1day (%) 2080s
CCCma-CanESM2	RegCM4-4	14.05	40.59
IPSL-CM5B-LR		16.52	39.31
GFDL-CM3		9.42	38.13
IPSL-IPSL-CM5A-MR	RCA4	30.83	35.47
MRI-CGCM3		27.29	33.91
CESM1-CAM5		29.20	33.35
ACCESS1-3		20.74	31.95
MPI-ESM-MR		10.05	31.19
IPSL-CM5A-LR		25.88	30.66
IPSL-IPSL-CM5A-LR	RegCM4-4	16.70	28.46
CanESM2		26.94	27.88
CMCC-CM		18.21	27.56
MIROC5		17.86	26.00
CCCma-CanESM2	RCA4	4.51	24.55
IPSL-CM5A-MR		20.26	24.02
MPI-M-MPI-ESM-LR	REMO2009	10.00	23.59
ICHEC-EC-EARTH	RCA4	4.38	23.29
MIROC-MIROC5	RCA4	6.36	21.51
CSIRO-QCCCE-CSIRO-Mk3-6-0	RCA4	23.18	20.72
MOHC-HadGEM2-ES	RCA4	19.73	20.36
CCSM4		19.86	19.38
bcc-csm1-1		20.60	18.10
CNRM-CERFACS-CNRM-CM5	RegCM4-4	16.54	17.84
ACCESS1-0		18.88	17.63
HadGEM2-ES		25.09	17.35
BNU-ESM		14.21	16.40
MPI-M-MPI-ESM-MR	RegCM4-4	10.67	16.10
HadGEM2-CC		16.67	16.02
NorESM1-M		4.43	15.49
NOAA-GFDL-GFDL-ESM2M	RCA4	13.62	15.36
GFDL-ESM2M		12.13	13.29
NOAA-GFDL-GFDL-ESM2M	RegCM4-4	5.50	12.37
NCC-NorESM1-M	RCA4	6.82	11.55
CNRM-CM5		-1.81	10.40
EC-EARTH		15.98	10.23
GFDL-ESM2G		0.12	9.90
HadGEM2-AO		6.93	9.45
MPI-ESM-LR		16.78	8.97
MIROC-ESM-CHEM		4.28	8.93
CNRM-CERFACS-CNRM-CM5	RCA4	9.24	8.84
bcc-csm1-1-m		17.73	8.36
inmcm4		4.03	6.45
MPI-M-MPI-ESM-LR	RCA4	8.93	5.53
MIROC-ESM		-11.46	5.24
CSIRO-QCCCE-CSIRO-Mk3-6-0	RegCM4-4	1.89	3.96
CSIRO-Mk3-6-0		-0.80	-1.63
CMCC-CMS		16.86	-8.92

Table 4: Values of the projected change in JJAS maximum RX1day averaged over Nepal under RCP8.5. The data is sorted based on the value of the projected change in the 2080s. CMIP5 GCM names are coloured based on their assessment category from Richardson (2021) and the RCM used to generate the regionally downscaled projections from CORDEX are included in the RCM column or left blank if a GCM projection.

GCM	RCM	Change in Rx1day (%) 2050s	Change in Rx1day (%) 2080s
IPSL-IPSL-CM5A-MR	RCA4	38.50	109.85
EC-EARTH		38.75	104.10
IPSL-CM5B-LR		57.77	100.31
GFDL-CM3		18.13	86.15
bcc-csm1-1		18.68	65.37
IPSL-CM5A-MR		33.17	62.06
CSIRO-QCCCE-CSIRO-Mk3-6-0	RCA4	36.46	60.67
MRI-CGCM3		28.33	60.35
CanESM2		16.45	54.15
CMCC-CM		24.56	53.90
ACCESS1-3		23.13	53.41
CESM1-CAM5		33.83	50.42
MIROC-MIROC5	RCA4	8.73	46.80
GFDL-ESM2M		39.73	46.28
CCCma-CanESM2	RegCM4-4	34.67	46.25
ACCESS1-0		20.59	45.51
HadGEM2-CC		18.46	44.82
GFDL-ESM2G		9.53	44.05
MIROC5		23.91	43.75
IPSL-IPSL-CM5A-LR	RegCM4-4	29.62	43.66
CCCma-CanESM2	RCA4	8.29	42.19
IPSL-CM5A-LR		31.67	41.56
MPI-M-MPI-ESM-LR	RCA4	11.93	41.47
HadGEM2-ES		19.85	39.59
BNU-ESM		27.44	38.05
MOHC-HadGEM2-ES	RCA4	25.82	36.11
NOAA-GFDL-GFDL-ESM2M	RegCM4-4	12.58	31.44
CCSM4		26.38	29.72
ICHEC-EC-EARTH	RCA4	25.00	27.95
NorESM1-M		15.07	27.69
NOAA-GFDL-GFDL-ESM2M	RCA4	5.83	25.80
MIROC-ESM-CHEM		30.60	24.19
NCC-NorESM1-M	RCA4	8.81	23.99
MPI-ESM-MR		0.28	21.91
CNRM-CM5		12.89	20.05
CMCC-CMS		12.88	19.77
bcc-csm1-1-m		8.76	19.11
MPI-ESM-LR		14.72	18.96
MPI-M-MPI-ESM-MR	RegCM4-4	8.85	18.32
CNRM-CERFACS-CNRM-CM5	RCA4	15.89	17.87
MPI-M-MPI-ESM-LR	REMO2009	9.34	14.39
CSIRO-Mk3-6-0		8.86	13.14
inmcm4		5.42	12.63
HadGEM2-AO		22.27	11.47
CNRM-CERFACS-CNRM-CM5	RegCM4-4	11.76	11.42
MIROC-ESM		-2.19	7.61
CSIRO-QCCCE-CSIRO-Mk3-6-0	RegCM4-4	2.50	6.40

References

Anandhi, A., Frei, A., Pierson, D. C., Schneiderman, E. M., Zion, M. S., Lounsbury, D., & Matonse, A. H. (2011). Examination of change factor methodologies for climate change impact assessment. *Water Resources Research*, *47*(3). https://doi.org/10.1029/2010WR009104

Beck, H. E., Wood, E. F., Pan, M., Fisher, C. K., Miralles, D. G., van Dijk, A. I. J. M., et al. (2019). MSWEP V2 Global 3-Hourly 0.1° Precipitation: Methodology and Quantitative Assessment. *Bulletin of the American Meteorological Society*, *100*(3), 473–500. https://doi.org/10.1175/BAMS-D-17-0138.1

Daron, J., Soares, M. B., Janes, T., Colledge, F., Srinivasan, G., Agarwal, A., et al. (2022). Advancing climate services in South Asia. *Climate Services*, *26*(July 2021), 100295. https://doi.org/10.1016/j.cliser.2022.100295

Duchon, J. (1977). Splines minimizing rotation-invariant semi-norms in Sobolev spaces. In *Constructive theory of functions of several variables* (pp. 85–100). Springer.

Giorgi, F., & Gutowski, W. J. (2015). Regional Dynamical Downscaling and the CORDEX Initiative. *Annual Review of Environment and Resources*, *40*(1), 467–490. https://doi.org/10.1146/annurev-environ-102014-021217

Hastie, T. J., & Tibshirani, R. J. (1990). *Generalized additive models* (Vol. Monographs). CRC press.

Hersbach, H., Bell, B., Berrisford, P., Biavati, G., Horányi, A., Muñoz Sabater, J., Nicolas, J., et al. (2018). ERA5 hourly data on pressure levels from 1979 to present. Copernicus Climate Change Service (C3S) Climate Data Store (CDS). https://doi.org/10.24381/cds.bd0915c6

IPCC. (2013). *Climate Change 2013: The Physical Science Basis. Contribution of Working Group I to the Fifth Assessment Report of the Intergovern-mental Panel on Climate Change*. [Stocker, T.F., D. Qin, G.-K. Plattner, M. Tignor, S.K. Allen, J. Boschung, A. Nauels, Y. Xia, V. Bex and P.M. Midgley (eds.)]: Cambridge University Press, Cambridge, United Kingdom and New York, NY, USA, 1535 pp.

IPCC. (2021). *Climate Change 2022: Impacts, Adaptation, and Vulnerability. Contribution of Working Group II to the Sixth Assessment Report of the Intergovernmental Panel on Climate Change*. (H.-O. Pörtner, D. C. Roberts, M. Tignor, E. S. Poloczanska, K. Mintenbeck, A. Alegría, et al., Eds.). Cambridge, UK: Cambridge University Press.

Kruschke, J. (2015). *Doing Bayesian Data Analysis: A Tutorial with R, JAGS, and Stan* (2nd ed.). Boston: Academic Press.

Maharjan, S. B., Steiner, J. F., Shrestha, A. B., Maharjan, A., Nepal, S., Shrestha, M. S., et al. (2021). *The Melamchi flood disaster: Cascading hazard and the need for multihazard risk management*. Lalitpur, Nepal: ICIMOD. https://doi.org/10.53055/ICIMOD.981

Miller, D. L., & Wood, S. N. (2014). Finite area smoothing with generalized distance splines. *Environmental and Ecological Statistics*, *21*(4), 715–731. https://doi.org/10.1007/s10651-014-0277-4

Pedersen, E. J., Miller, D. L., Simpson, G. L., & Ross, N. (2019). Hierarchical generalized additive models in ecology: an introduction with mgcv. *PeerJ*, *7*, e6876. https://doi.org/10.7717/peerj.6876

Rajbhandari, R., Shrestha, A. B., Nepal, S., & Wahid, S. (2016). Projection of Future Climate over

the Koshi River Basin Based on CMIP5 GCMs. *Atmospheric and Climate Sciences*, *06*(02), 190–204. https://doi.org/10.4236/acs.2016.62017

Ramsay, T. O., Burnett, R. T., & Krewski, D. (2003). The effect of concurvity in generalized additive models linking mortality to ambient particulate matter. *Epidemiology*, *14*(1), 18–23.

Rani, S. I., T, A., George, J. P., Rajagopal, E. N., Renshaw, R., Maycock, A., et al. (2021). IMDAA: High Resolution Satellite-era Reanalysis for the Indian Monsoon Region. *Journal of Climate*, 1–78. https://doi.org/10.1175/JCLI-D-20-0412.1

Richardson, K. J. (2021). *Understanding and quantifying extreme precipitation events in South Asia: Part II - Process-based evaluation of climate model simulations for South Asia*. Exeter, UK.

Scaife, A. A., Camp, J., Comer, R., Davis, P., Dunstone, N., Gordon, M., et al. (2019). Does increased atmospheric resolution improve seasonal climate predictions? *Atmospheric Science Letters*, *20*(8), e922. https://doi.org/10.1002/asl.922

Shirsat, T. S., Kulkarni, A. V., Momblanch, A., Randhawa, S. S., & Holman, I. P. (2021). Towards climate-adaptive development of small hydropower projects in Himalaya: A multi-model assessment in upper Beas basin. *Journal of Hydrology: Regional Studies*, *34*, 100797. https://doi.org/10.1016/j.ejrh.2021.100797

Shrestha, A., Shrestha, S., Tingsanchali, T., Budhathoki, A., & Ninsawat, S. (2021). Adapting hydropower production to climate change: A case study of Kulekhani Hydropower Project in Nepal. *Journal of Cleaner Production*, *279*, 123483. https://doi.org/10.1016/j.jclepro.2020.123483

Steptoe, H. (2022). *Understanding and quantifying extreme precipitation events in South Asia: Part III - Observational datasets for the assessment of present day monsoon-season rainfall extremes in Nepal*. Exeter, UK.

Taylor, K. E., Stouffer, R. J., & Meehl, G. A. (2012). An overview of CMIP5 and the experiment design. *Bulletin of the American Meteorological Society*, *93*(4), 485–498. https://doi.org/10.1175/BAMS-D-11-00094.1

Volodin, E. M., Dianskii, N. A., & Gusev, A. V. (2010). Simulating present-day climate with the INMCM4.0 coupled model of the atmospheric and oceanic general circulations. *Izvestiya, Atmospheric and Oceanic Physics*, *46*(4), 414–431. https://doi.org/10.1134/S000143381004002X

Wang, X., Tolksdorf, V., Otto, M., & Scherer, D. (2021). WRF-based dynamical downscaling of ERA5 reanalysis data for High Mountain Asia: Towards a new version of the High Asia Refined analysis. *International Journal of Climatology*, *41*(1), 743–762. https://doi.org/10.1002/joc.6686

Wijngaard, R. R., Lutz, A. F., Nepal, S., Khanal, S., Pradhananga, S., Shrestha, A. B., & Immerzeel, W. W. (2017). Future changes in hydro-climatic extremes in the Upper Indus, Ganges, and Brahmaputra River basins. *PLOS ONE*, *12*(12), e0190224. https://doi.org/10.1371/journal.pone.0190224

Wood, S. N. (2003). Thin-plate regression splines. *Journal of the Royal Statistical Society (B)*, *65*(1), 95–114.

Wood, S. N. (2017). *Generalized Additive Models: An Introduction with R* (2nd ed.). Chapman and Hall/CRC.

Wood, S. N. (2020). Inference and computation with generalized additive models and their

extensions. *TEST*, *29*(2), 307–339. https://doi.org/10.1007/s11749-020-00711-5

Yatagai, A., Kamiguchi, K., Arakawa, O., Hamada, A., Yasutomi, N., & Kitoh, A. (2012). APHRODITE: Constructing a Long-Term Daily Gridded Precipitation Dataset for Asia Based on a Dense Network of Rain Gauges. *Bulletin of the American Meteorological Society*, *93*(9), 1401–1415. https://doi.org/10.1175/BAMS-D-11-00122.1

Met Office
FitzRoy Road
Exeter
Devon
EX1 3PB
United Kingdom